ELSEVIER Applied Mathematics and Computation 101 (1999) 159–207

APPLIED MATHEMATICS AND COMPUTATION

A numerical study of an ill-posed Boussinesq equation arising in water waves and nonlinear lattices: Filtering and regularization techniques [1]

Prabir Daripa *, Wei Hua

Texas A&M University, Department of Mathematics, College Station, TX 77843, USA

Abstract

We consider an ill-posed Boussinesq equation which arises in shallow water waves and nonlinear lattices. This equation has growing and decaying modes in the linear as well as nonlinear regimes and its linearized growth rate σ for short-waves of wavenumber k is given by $\sigma \sim k^2$. Previous numerical studies have addressed numerical difficulties and construction of approximate solutions for ill-posed problems with short-wave instability up to $\sigma \sim k$, e.g. Kelvin–Helmholtz ($\sigma \sim k$) and Rayleigh–Taylor ($\sigma \sim \sqrt{k}$) instabilities. These same issues are addressed and critically examined here for the present problem which has more severe short-wave instability. In order to develop numerical techniques for constructing good approximate solutions of this equation, we use a finite difference scheme to investigate the effect of this short-wave instability on the numerical accuracy of the exact solitary wave solution of this equation. Computational evidence is presented which indicates that numerical accuracy of the solutions is lost very quickly due to severe growth of numerical errors, roundoff as well as truncation. We use both filtering and regularization techniques to control growth of these errors and to provide better approximate solutions of this equation. In the filtering technique, numerical experiments with three types of spectral filters of increasing order of regularity are performed. We examine the role of regularity of these filters on the accuracy of the numerical solutions. Numerical evidence is provided which indicates that the regularity of a filter plays an important role in improving the accuracy of the solutions. In the regularization technique, the ill-posed equation is regularized by adding a higher

* Corresponding author.

[1] This research was supported by NSF grants No. DMS–9208061 and by the Office of the Vice President for Research and Associate Provost for Graduate Studies at Texas A&M University.

PII: S0096-3003(98)10070-X

order term to the equation. Two types of higher order terms are discussed: (i) one that diminishes the growth rate of all modes below a cutoff wavenumber and sets the growth rate of all modes above it to zero; and (ii) the other one diminishes the growth rate of all modes and the growth rate asymptotically approaches to zero as the wavenumber approaches infinity. We have argued in favor of the first type of regularization and numerical results using a finite difference scheme are presented. Numerical evidence is provided which suggests that regularization in combination with the most regular (C^2 here) spectral filter for small values of the regularization parameter can provide good approximate solutions of the ill-posed Boussinesq equation for longer time than possible otherwise. Some of the ideas presented here can possibly be utilized for solving other ill-posed problems with severe short-wave instabilities and may have an important role to play in numerical studies of their solutions.

Keywords: Ill-posed problem; Boussinesq equation; Solitary wave; Water waves; Finite difference equation

1. Introduction

In this paper, we are interested in the numerical study of the ill-posed Boussinesq equation

$$u_{tt} = (p(u))_{xx} + u_{xxxx}, \tag{1.1}$$

with $p(u) = u + u^2$ and subject to some restricted class of initial data, $u(x,0)$ and $u_t(x,0)$ to be discussed later. The corresponding linearized PDE has decaying as well as growing modes, $e^{\sigma t + ikx}$, with the dispersion relation about a constant state, u_c, given by

$$\sigma_{\mp} = \mp k\sqrt{k^2 - p'(u_c)}. \tag{1.2}$$

Without any loss of generality, we have used waves with wavelength 2π in the dispersion relations. (Thus, the wavenumber k in Eq. (1.2) actually refers to $(2\pi/L)k$ whenever this problem is considered in a domain of length L.) The equilibrium states in the elliptic region (i.e. $p'(u_c) = 1 + 2u_c < 0$) are unstable to all modes and the states in the hyperbolic region are unstable to modes $|k| > \sqrt{p'(u_c)}$. Since the growth rate, i.e. the real part of σ_+, is a monotonically increasing function of the wavenumber, there is no wavenumber with maximal rate of stability. According to the dispersion relation (1.2) short-wave instability is given by

$$\sigma \approx k^2 \quad \text{as } k \to \infty. \tag{1.3}$$

It should be noted that the well-posed Boussinesq equation differs from Eq. (1.1) only in the sign of the term containing u_{xxxx}. The well-posed equation is easy to solve numerically [9] and does not concern us in this paper. More-

over, we are interested only in the hyperbolic regime of this equation and thus we are not interested in this paper numerical issues in the subcritical (i.e. $p'(u_c) = 1 + 2u_c < 0$) or critical regimes (i.e. $p'(u_c) = 1 + 2u_c = 0$).

Difficulty in solving the ill-posed equation (1.1), analytically and numerically, arises due to severe short-wave instability (1.3). In general, classical solutions of this equation with arbitrary initial data are not expected to exist for positive time except for some special choices of initial data. Using inverse scattering technique, Deift et al. [4] have implicitly constructed solutions of Eq. (1.1) without the term u_{xx}, some global and some that blow up in finite time. (The term u_{xx} in Eq. (1.1) can be removed by replacing u by $u - \frac{1}{2}$.) Except for arbitrary constants, only other C^∞ solutions known to exist for this equation are of soliton-type (singlet as well as doublet) [5,10]. The solitary wave solution is given by [5,10]

$$u^s(x,t) = A\,\mathrm{sech}^2\left\{\sqrt{A/6}(x - ct + x_0)\right\} + \left(b - \frac{1}{2}\right), \tag{1.4}$$

where A is the amplitude of the solitary wave, b is a free parameter and $c = \mp\sqrt{2(b + A/3)}$ is the speed of the solitary wave. Solitary wave corresponding to $b = \frac{1}{2}$ and $x_0 = 0$ which are convenient for numerical purposes in this paper is given by

$$u^s(x,t) = A\,\mathrm{sech}^2\left\{\sqrt{A/6}(x - ct)\right\}. \tag{1.5}$$

The ill-posed Boussinesq equation (1.1) commonly describes propagation of small amplitude long waves (long compared to the amplitude of the wave) in several physical contexts including shallow water under gravity [16] and one dimensional nonlinear lattices [17]. Asymptotic expansion of appropriate physical equations in some small parameter in k usually gives rise to the ill-posed Boussinesq equation within some order of approximation. For example, in Appendix A we describe briefly from Ref. [16] the origin of this equation in the context of shallow water waves. Usually, as in the case of water waves, this equation is physically relevant only for small k and breaks down for large k. Therefore severe growth rate of waves with large k may not appear to be an important issue. However, these short-waves will enter into the calculation due to numerical error as well as due to nonlinearity of the equation. Therefore accurate computation of even physically relevant solutions of this equation is not possible without circumventing numerical difficulties due to this short-wave instability. The truncation and roundoff errors during machine computations introduce spurious perturbations at all scales, small and large. These small scale perturbations which grow very rapidly cause significant difficulty in constructing good approximate solutions of this equation. Such difficulties also occur for other ill-posed problems such as Kelvin–Helmholtz instability [7] and Rayleigh–Taylor instability [2]. However, short-wave instabilities are less

severe for these ($\sigma \sim \sqrt{k}$ for Kelvin–Helmholtz and $\sigma \sim k$ for Rayleigh–Taylor) cases. Therefore it is somewhat more challenging and interesting to asses the level of numerical difficulties that this severe short-wave instabilities pose. Our aim in this paper is to explore ways to circumvent these difficulties in order to obtain good approximate solutions of this equation subject to appropriate initial data. Hope is that this will allow further numerical studies of this and other severely ill-posed equations and their solutions.

It may be worth mentioning here that, in the weakly nonlinear limit, shallow water wave equation (A.7) for long waves (see Appendix A) reduces to the well known Korteweg–de Vries (KdV) equation [16]

$$u_t + uu_x + u_{xxx} = 0. \tag{1.6}$$

The difference between this equation and the Boussinesq equation is that the latter allows bidirectional waves while KdV only unidirectional waves.

At this point we would like to mention a loose analogy between Boussinesq equations (ill-posed as well as well-posed) and isothermal equations of fluid flows [12,13]. The Boussinesq equation (1.1) can be viewed as a degenerate case of the following 2×2 system of first order equations with $\epsilon = 0$ and $\delta = -1$,

$$u_t - v_x = 0, \quad v_t - (p(u))_x = \delta u_{xxx} + \epsilon v_{xx}. \tag{1.7}$$

This system describes isothermal fluid flows with specific volume u, velocity v, pressure law $p(u)$, viscosity coefficient ϵ and capillary coefficient δ [12,13]. Therefore, Boussinesq equations also describe the isothermal inviscid fluid flow in one dimension with quadratic pressure law and a capillarity coefficient which is positive for the well-posed Boussinesq equation ($\delta = 1$) and negative for the ill-posed Boussinesq equation ($\delta = -1$). The ill-posedness of Eq. (1.1) can be viewed as a result of this negative capillarity. It should not be confused with the surface tension effect in the context of water waves. As discussed before and in Appendix A, the ill-posed Boussinesq equation arises out of asymptotic expansion of shallow water equations which contain no surface tension effect (see also [16]). The system (1.7) with positive capillary coefficient and various cubic pressure laws including van der Waals pressure law has been studied as models of dynamic phase transition by Affouf and Caflisch [1] and Slemrod [12,13] among others. The hyperbolic region of the quadratic pressure law of the Boussinesq system has the same qualitative feature as the van der Waals pressure law at high enough temperature. It appears that the Boussinesq system due to its exact soliton-type solutions and simplicity may be useful in numerical study of conservation laws of mixed type.

The ill-posed Boussinesq equation (1.1) which arises in various contexts as discussed above may not always have a sound physical basis for explaining phenomena at small scales. However, we believe that mathematical and com-

putational difficulties associated with the study of this equation can be more generic than it appears to be and may occur in other physical and mathematical contexts. Moreover, numerical methods which will allow construction of good approximate solutions of such severely ill-posed problems are not known and are not easy to construct without proper understanding of the effect of such short-wave instability on the accuracy of the numerical solutions. The Boussinesq equation (1.1) provides a simple case of severely ill-posed nonlinear problems which also has exact traveling wave solutions. These exact solutions can be used during machine computations to develop appropriate numerical methods that can be useful not only for solving this equation but possibly other ill-posed problems as well. Numerical experiments can then possibly be performed with these numerical methods to investigate further the mathematical properties of this and other similar imposed problems.

The paper is laid out as follows. In Section 2 we present a finite difference scheme which is second order accurate in time and space. We present a linearized stability analysis of this scheme and derive its dispersion relation. Mesh sizes based on good approximation of the analytical dispersion relation by the numerical one are obtained. These mesh sizes are then used in single and double precision calculation and results are presented to show the dangerous effect of machine roundoff error on the accuracy of numerical solutions. We compute error estimates of the numerical solutions to provide numerical evidence of convergence of the numerical schemes. In Section 3, we apply the numerical scheme with three filters of increasing order of regulatory to show that the spurious errors introduced by finite digit arithmetics of machine computation can be controlled to a considerable extent by appropriate choice of filters. We present a new filter which is twice continuously differentiable and present in detail application procedure of this filter. Numerical results with this filter are presented to justify its usefulness in the numerical construction of approximate solutions of ill-posed problems. In Section 4, we present viscosity-like and surface-tension like regularization techniques by adding higher order terms to Eq. (1.1). We carry out their linearized stability analysis and derive their dispersion relations. There we argue based on linearized stability analysis and physical consideration that surface-tension-like regularization is more appropriate and is likely to give better approximate solution. Moreover, it is easier to implement surface-tension-like regularization than the viscosity-like regularization. The numerical scheme of Section 2 is then extended for the regularized equation with surface-tension-like regularization. Linearized stability analysis of this scheme is carried out and numerical results with this scheme are presented. We find that these numerical solutions for modest values of regularizing parameters can also provide very good approximations to solutions of the ill-posed Boussinesq equation (1.1). In Section 5, we summarize and discuss our findings and mention some problems which are areas of future research.

2. Numerical scheme

2.1. Finite difference scheme

Eq. (1.1) is solved numerically in a finite domain, $a \leqslant x \leqslant b$, for $t > 0$. We use finite difference method with uniform grid spacings h in x and τ in t. Using v_j^n to denote the approximate value of $u(x,t)$ at $x = a + jh,\ t = n\tau$ and using usual finite difference operators D^+ and D^- to denote forward and backward differences, Eq. (1.1) can be approximated by the Finite Difference Equation (FDE).

$$\frac{D_t^+ D_t^- v_j^n}{\tau^2} = \frac{D_x^+ D_x^-(p(v_j^n))}{h^2} + \frac{(D_x^+ D_x^-)^2(v_j^{n+1} + v_j^{n-1})}{2h^4}, \tag{2.1}$$

for $\tau > 0$ and $0 < j < N (0 \leqslant j < N$ in case of periodic domain) where $b - a = Nh$. The truncation error is $E(h,\tau) = \mathrm{O}(h^2) + \mathrm{O}(\tau^2)$.

Following Affouf and Caflisch [1], we use the following fourth order accurate boundary conditions to estimate boundary conditions $v(a-h, n\tau)$ and $v(b+h, n\tau)$, for $n \geqslant 0$.

$$v(a-h,n\tau) = -\frac{3}{2}v(a,n\tau) + 3v(a+h,n\tau) - \frac{1}{2}v(a+2h,n\tau) - 3v'(a,n\tau)h, \tag{2.2}$$

$$v(b+h,n\tau) = -\frac{3}{2}v(b,n\tau) + 3v(b-h,n\tau) - \frac{1}{2}v(b-2h,n\tau) + 3v'(b,n\tau)h \tag{2.3}$$

and the following third order accurate initialization to estimate $v(jh,\tau),\ 0 \leqslant j \leqslant N$

$$v(.,\tau) = v(.,0) + v'(.,0)\tau + v''(.,0)\frac{\tau^2}{2} + \mathrm{O}(\tau^3), \tag{2.4}$$

where $v(.,\tau)$ and $v'(.,\tau)$ are given, and $v''(.,\tau)$ can be obtained directly from using the Boussinesq equation (1.1).

We computed numerical solutions in the interval (a,b) with $a = -128,\ b = 128$, subject to the following initial conditions

$$u(x,0) = u^{\mathrm{s}}(x,0), \qquad u_t(x,0) = u_t^{\mathrm{s}}(x,0) \tag{2.5}$$

and the boundary conditions

$$u(a,t) = u^{\mathrm{s}}(a,t), \qquad u(b,t) = u^{\mathrm{s}}(b,t), \quad t > 0, \tag{2.6}$$

where $u^{\mathrm{s}}(x,t)$ is given by (1.5). The computations were performed in single (7 digit arithmetic) and double (15 digit arithmetic) precisions. Below we often use the notations 'sp' for 'single precision' and 'dp' for 'double precision'.

Our choice of the computational domain $(-128,\ 128)$ allows the physical boundaries to be well-away from the support of the solitary wave so that approximate numerical solutions remain almost periodic within machine precision. The lack of periodicity of the numerical solutions or/and the inappropriateness of the use of Fourier filtering are not relevant issues during the relatively short time intervals of computation that are involved here. This, in a way, is very convenient as it allows us to focus solely on the numerical difficulties associated with the severe short wave instability of this problem. The numerical results that are reported in this paper involve time interval during which the movement of the solitary wave is so small compared to the computational interval that the approximate numerical solutions reported here remain periodic within an error of the size of the machine precision. Therefore Fourier filtering that we use in Section 3 remains appropriate for all our computations in this paper.

2.2. Linearized stability of the FDE about any constant state u_c.

Any constant state, $u = u_c$, is a solution to both the PDE and the FDE. Denoting the perturbation about the constant state, u_c, by $\tilde{v}_j^n$, and then linearizing the FDE about this constant state we obtain

$$\frac{D_t^+ D_t^- \tilde{v}_j^n}{\tau^2} = (p'(u_c))\frac{D_x^+ D_x^- \tilde{v}_j^n}{h^2} + \frac{(D_x^+ D_x^-)^2(\tilde{v}_j^{n+1} + \tilde{v}_j^{n-1})}{2h^4}. \tag{2.7}$$

With $\tilde{v}_j^n = \rho^n e^{i\xi j}$ in Eq. (2.7) (where $\rho = e^{\beta\tau}$, $\xi = kh$, k is the wavenumber and real part of β is the growth rate), the dispersion relation for the numerical scheme is

$$\left(1 - 8r^2 \sin^4\frac{\xi}{2}\right)\rho^2 + 2\left(2\lambda^2 p'(u_c)\sin^2\frac{\xi}{2} - 1\right)\rho + \left(1 - 8r^2\sin^4\frac{\xi}{2}\right) = 0, \tag{2.8}$$

where $r = \tau/h^2$ and $\lambda = \tau/h$.

The dispersion relations (1.2) for the linearized Boussinesq equation and Eq. (2.8) for the linearized FDE are qualitatively similar in the sense that there are neutral, growing and decaying modes in both the FDE and the PDE if u_c, h and τ satisfy the following relations:

$$\lambda^2 \leqslant \frac{1}{p'(u_c)} \quad \text{and} \quad r < \frac{1}{2\sqrt{2}}. \tag{2.9}$$

The first of these conditions is the usual CFL condition which ensures that the numerical scheme has only decaying modes in the absence of u_{xxxx} term in Eq. (1.1). This is consistent with the corresponding exact dispersion relation, i.e. Eq. (1.2) without the k^2 term. The second of these condition is slightly stringent than the usual stability condition, $r < \frac{1}{2}$, associated with the numerical

scheme for the parabolic heat equation. Eq. (1.1) without the hyperbolic term is a higher order parabolic equation than the heat equation and it has stable as well as unstable modes (see Eq. (1.2)). The condition $r < \frac{1}{2}$ ensures that our numerical scheme without the hyperbolic term will also have stable and unstable modes. Modes with infinite growth/decay rate are allowed by the requirement $r < \frac{1}{2}$. We prefer to avoid these modes. This is accomplished by making this criterion more stringent as in Eq. (2.9). For our later numerical purposes it is convenient to rewrite Eq. (2.9) in terms of τ and h.

$$h \leqslant \frac{2\sqrt{2}}{\sqrt{p'(u_c)}} \quad \text{and} \quad \frac{\tau}{h^2} < \frac{1}{2\sqrt{2}}. \tag{2.10}$$

Numerical scheme (2.1) should preferably use values of grid sizes τ and h which satisfy (2.10) allow discrete dispersion relation, i.e. the plot of growth rate $\ln|\rho|/\tau$ versus the wavenumber k, best approximate the continuous dispersion relation over as wide range of the spectrum as possible. Fig. 1 shows the plot of growth rate versus the wavenumber for the PDE and FDE for several choices of h and τ all of which are consistent with inequalities (2.9). In our numerical experiments below $u(x)$ takes values between 0.0 and 0.5 for all x. The value of u_c in this range has little effect on the dispersion relation. Fig. 1 shows the case when $u_c = 0.0$. The plot for the case when $u_c = 0.5$ is almost identical. Eq. (1.1) remains hyperbolic for values of u in this range.

Fig. 1 shows that agreement between theoretical and numerical dispersion relations is better with $\tau = 0.085$ than with much smaller time step $\tau = 0.01$ with a mesh spacing size $h = 0.5$. Numerical solutions at time level $t = 1$ for these choices of τ are compared against the exact solutions at the same time level in Fig. 2. Numerical results have been obtained in double digit arithmetics so that the roundoff error is negligible. Fig. 2 shows that numerical results with

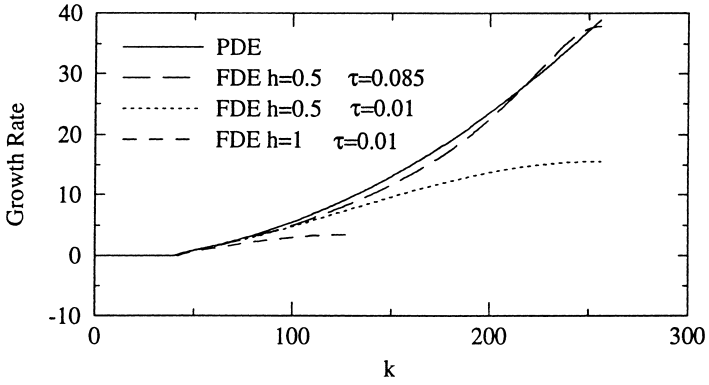

Fig. 1. Dispersion relation for the PDE and FDE: growth rate $\ln|\rho|/\tau$ versus wavenumber k for three choices of h and τ when $u_c = 0.0$.

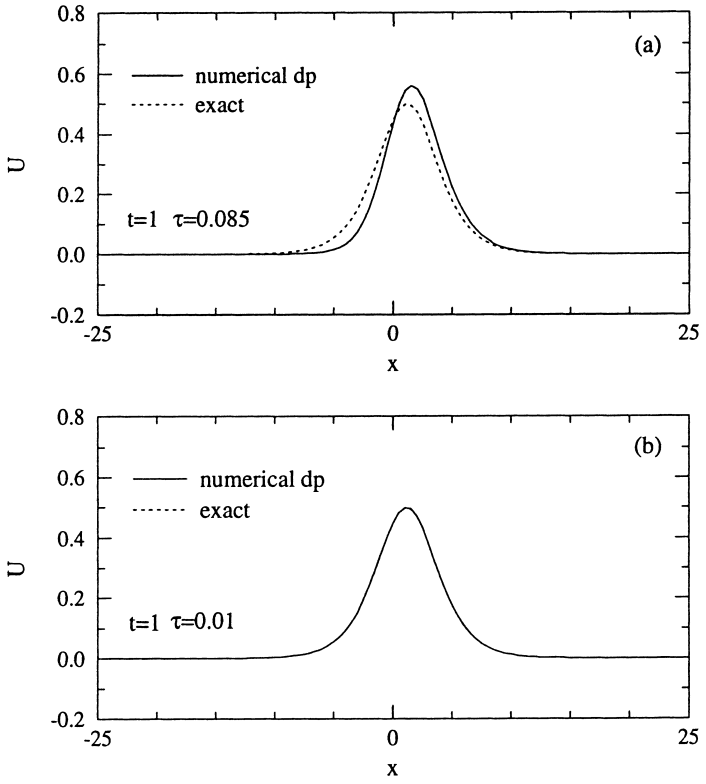

Fig. 2. Comparison of numerical and exact solutions at the time level $t = 1$. The calculations were done in double precision (15 digit arithmetics) with $h = 0.5$ and time step sizes (a) $\tau = 0.085$; (b) $\tau = 0.01$.

smaller time step are better than the ones with the larger time step even though the numerical dispersion relation corresponding to the larger time step better approximates the exact numerical dispersion relation (see Fig. 1). Many other computations with these time step sizes also support this observation. This seemingly paradoxical behavior has a very simple explanation: time integration of large truncation error associated with the larger time step size more than offsets any advantage in accuracy offered by the superior dispersion relation.

2.3. Linearized growth of truncation and roundoff errors

Here we adopt the analysis similar to that of Krasny [7]. Under the dynamics of the numerical scheme (2.1), an error of magnitude $a(0)$ in a Fourier mode with wavenumber k linearly grows to $a(t)$ in time t given by

$$t = \frac{1}{\omega(t)} \ln \frac{a(t)}{a(0)}, \tag{2.11}$$

where $\omega(t)$ is the linearized growth rate of the Fourier mode. For appropriate choices of h and τ, the numerical dispersion relation can be approximated by

$$\omega(k) = c(k)k^2, \tag{2.12}$$

where $c(k)$ is some function of k. For $c(k) \sim 1$ as $k \to \infty$, we have the linearized dispersion relation of the PDE in this limit. If $a(0) = 10^{-d}$ and $a(t_1) = 10^{-p}$ for the fastest growing Fourier mode in the numerical scheme, then it follows from Eq. (2.11) and Eq. (2.12) that

$$t_1 \sim \left(\frac{h}{\pi}\right)^2 (d-p) \ln 10, \tag{2.13}$$

where we have used $k = O(N/2)$, the wavenumber of fastest growing mode participating in the numerical scheme with N number of grid points, and $c(k) \sim 1$ due to moderately good agreement between numerical and exact dispersion relations for certain choices of h and τ in Fig. 1. Similar arguments would give $t_1 \sim O(h)$ for KH (see also [7]), and $t_1 \sim O(\sqrt{h})$ for RT types of instabilities. The arguments leading up to Eq. (2.13) here is similar to that used by Krasny [7] for KH instability.

Eq. (2.13) shows that errors in the high wavenumber mode grow more rapidly with decreasing mesh sizes. Such severe growth or error in the high wave number modal amplitudes can cause significant loss of numerical accuracy in the computed solutions as seen in Fig. 3. For example, an initial error of magnitude 10^{-7} (such errors are likely in single precision calculation) will increase to a value of $10^{-5.5}$ in a single time step when $\tau = 0.085$ and $h = 0.5$, the parameter values corresponding to numerical dispersion relation that best approximates the exact dispersion relation (see Fig. 1). In reality, this error can be even larger due to nonlinear ill-posedness of the Boussinesq equation. Such an amplification of machine roundoff error in a single time step can cause serious difficulties in advancing the solutions correctly any further. Therefore the time step sizes must be chosen smaller than this so that postprocessing of data after each or few time steps will make it possible to reduce the spurious effects of roundoff error. A smaller choice of τ, of course, entails a tradeoff between the error in the numerical solution due to disagreement between numerical and theoretical dispersion relations and the error in the numerical solution due to catastrophic growth of spurious errors in a single time step. Below we exemplify in some detail the numerical difficulties due to short-wave instabilities.

The results in Fig. 3 shows the effect of roundoff error on the numerical accuracy of the solution (here the effect of truncation error on the solution is kept negligibly small by integrating the solution for short time). Fig. 3(a) and 3(b) show numerical and exact solutions at the time level $t = 1$ with mesh sizes $h = 1$ and $h = 0.5$ respectively. Numerical computations have been performed

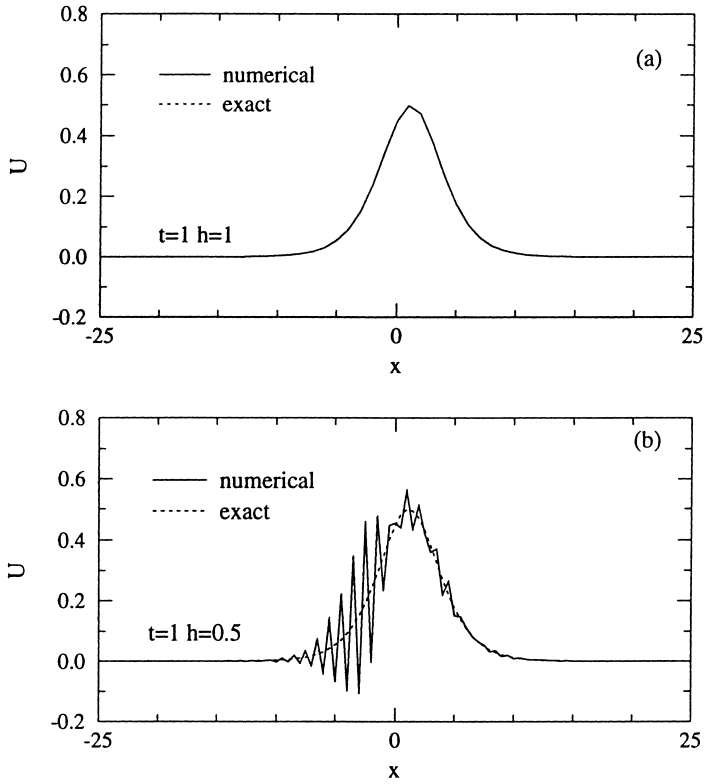

Fig. 3. Comparison of numerical and exact solutions at the time level $t = 1$. The calculations were done in single precision (7 digit arithmetics) with different mesh size (a) $h = 1$; (b) $h = 0.5$.

in single precision. We see in these plots that very accurate solutions are obtained with $h = 1.0$ suggesting that the effect of truncation error on the solution at $t = 1$ is small. The effect of truncation error on the numerical solution at $t = 1$ is even smaller with smaller time step size $h = 0.5$ in Fig. 3(b). However, these figures show that numerical solutions get even worse with small time step size $h = 0.5$ even though the truncation error is smaller. Smaller mesh size here causes participation of higher wavenumber modes. Short-wave instability causes rapid growth of spurious perturbations in these mode introduced by roundoff errors resulting in severe deterioration of numerical solutions as seen in this figure. In general, any gain in the accuracy of numerical solutions due to smaller mesh sizes is quickly lost due to these instabilities. This brings computations to a halt sooner or later depending on the mesh size and the machine precision used.

The truncation error can cause significant loss in the accuracy of numerical solutions when calculations are carried out for longer time. For example,

advancing the numerical solution in Fig. 3(a) further deteriorates the accuracy of the numerical solution in Fig. 4(a) and higher machine precision calculation does not improve the solution either as seen in Fig. 4(b). In fact, numerical solutions obtained in single (Fig. 4(a)) and double (Fig. 4(b)) precision calculations appear to be almost the same. This is due to the fact that the deteriorating effect of roundoff error on the accuracy of numerical solutions in single precision calculation is almost negligible compared to that of the truncation error. Also notice in Fig. 4(c) that all Fourier modes participating in the calculations here have amplitudes greater than the roundoff error of single precision calculation.

Above example does not show that calculations on a higher precision machine can improve the accuracy of numerical solutions. This is due to the fact that roundoff error is not the cause of inaccuracies in numerical solution at $t = 3.5$ in Fig. 4.

The inaccuracies in the numerical solution shown in Fig. 3(b) is due to roundoff error as discussed earlier and can be considerably improved with higher precision calculation as seen in Fig. 5(a) and 5(b). Fig. 5(a) and 5(b) compare numerical solutions obtained in single and double precisions respectively with mesh size $h = 0.5$. Fig. 5(c) shows that all participating modes have amplitudes greater than roundoff error of double precision (15 digit arithmetics) calculations and approximately half of these participating modes with high wavenumber have amplitudes less than the roundoff error of single precision (7 digit arithmetics) calculations. Therefore, initial amplitudes of these high wavenumber modes are severely contaminated with spurious perturbations introduced by machine roundoff error in single precision calculations. Such contamination is relatively much less in double precision calculation as is evident from Fig. 5(c).

In summary, Figs. 3–5 show that numerical construction of good approximate numerical solutions for long time requires proper control of truncation as well as roundoff errors. We have seen and argued above that as we keep refining the mesh size, truncation error becomes less of a problem and roundoff error becomes more of a serious problem to the construction of a good approximate solution. In other words, growth rate of short waves restricts the accuracy of numerical solutions that can be obtained from finite precision machine calculations. Unless the data are perturbed so as to suppress the spurious effects of roundoff error or the dispersion relation is modified in a clever way, computation of good approximations to long-time solutions is difficult. According to Tikhonov and Arsenin [14], the first of these methods is known as filtering method and the second of these methods is known as regularization method. Before we discuss, implement and show the performance of these methods in the Sections 3 and 4, we provide numerical evidence of convergence of the numerical scheme (2.1) in the following section.

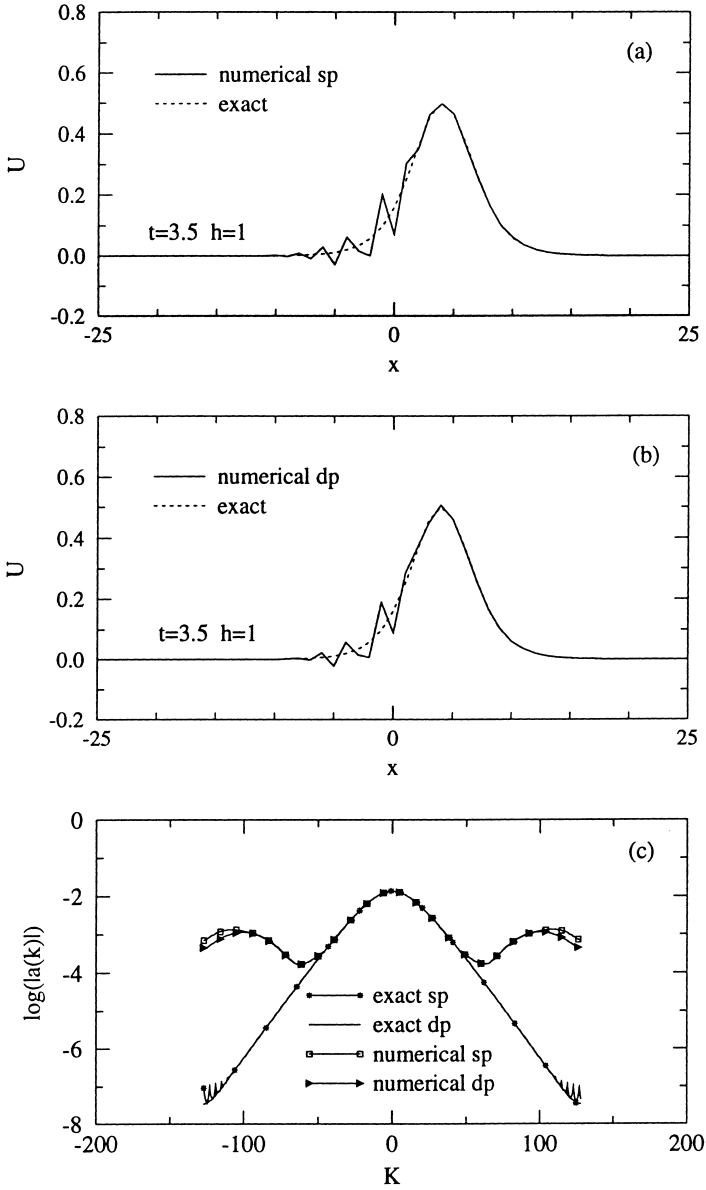

Fig. 4. Comparison of numerical and exact solutions at the time level $t = 3.5$. The calculations were done in (a) *single precision* (7 digit arithmetics); (b) *double precision* (15 digit arithmetics) with $h = 1$ and $\tau = 0.01$. (c) $\log_{10}|a_k|$ versus k where $|a_k|$ is the amplitude of the Fourier mode with wavenumber k.

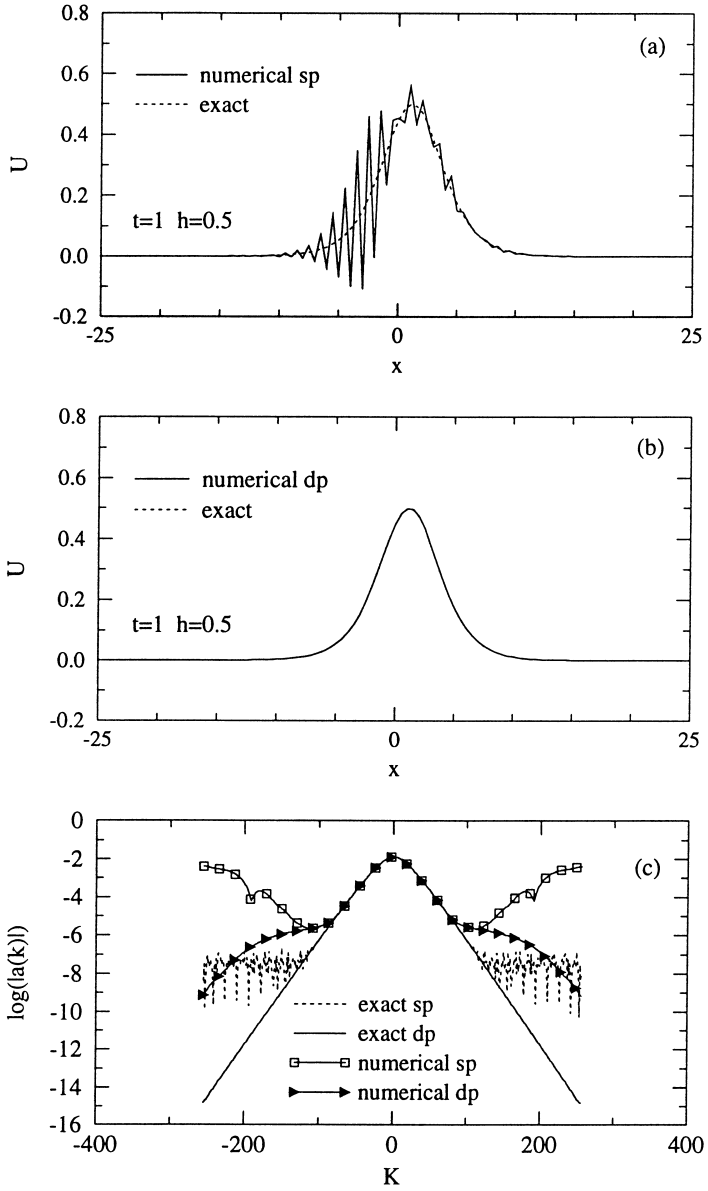

Fig. 5. Comparison of numerical and exact solutions at the time level $t = 1$. The calculations were done in (a) *single precision* (7 digit arithmetics); (b) *double precision* (15 digit arithmetics) with $h = 0.5$ and $\tau = 0.01$. (c) $\log_{10}|a_k|$ versus k where $|a_k|$ is the amplitude of the Fourier mode with wavenumber k.

2.4. Numerical evidence of convergence of the numerical scheme (2.1)

A consequence of the short-wave instability of the numerical scheme (2.1) is that the scheme is linearly unstable. Linearly unstable numerical methods for non-linear ill-posed problems may, however, converge. For example point vortex method for the vortex sheet problem, even though unstable, converges up to the time of singularity formation (see [6]). Therefore it makes sense to investigate whether the scheme (2.1) converges or not so that we have some confidence in the numerical results presented in this work.

We have seen that spurious error introduced by machine roundoff error increases with decreasing mesh size. Therefore, it is difficult to numerically investigate whether the numerical scheme converges or not under mush refinement unless we either find a way to completely eliminate the roundoff error or study the convergence issues up to a mesh size which is large enough not to cause any significant roundoff error and then extrapolate the behavior of the error in the limit of zero mesh size. The first method, i.e. complete elimination of roundoff error regardless of the mesh size, is not practical when computations are carried out on finite precision machines and/or algorithms. The second method involves studying the error in the numerical solution as a function of mesh size until mesh size is small enough to cause severe growth of spurious perturbations introduced by roundoff error. Therefore right at the outset we must emphasize the experimental nature of this investigation. One can at best draw inferences from numerical data whether the scheme converges or not from this study. Even though this is not a rigorous proof of convergence of the numerical scheme, we believe that it is worth presenting the results of such a numerical study of the convergence issue.

Numerical estimates of L_2 and L_∞ errors obtained in single and double precision computations are shown in Tables 1 and 2. Table 1 shows these errors only up to $t = 0.8$ because inaccuracies in the numerical solutions due to short-wave instabilities seem to be insignificant up to $t \sim 0.8$ at which time this error starts affecting the accuracy of the numerical solutions. In fact, some deterioration in the convergence is already evident in this table at $t = 0.4,\ 0.6,\ 0.8$ when $h = 0.5$, indicating the spurious effects of short-wave instabilities rather than failure of convergence of the numerical scheme. This is borne out by the values of these error estimates in Table 2 where calculations are done in double precision. The deteriorating effects of the severe short-wave instabilities on the convergence properties is now felt only at $t = 0.8$ when $h = 0.5$ as seen in this table. Even though accurate computations can be carried out for longer time, we have shown these estimates up to the same time level as that in Table 1 for making a relative comparison of accuracies between single and double precision calculations. We believe there is enough evidence here which lead us to conjecture that scheme (2.1) converges for, at least, some finite time.

Table 1
The L_2 and L_∞ error estimates of numerical solutions with $\tau = 0.01$ and different mesh size computed in *single* precision without using any filter

Time	h	L_2	L_∞
0.2	4	9.08077E − 04	1.01055E − 03
	2	2.00957E − 04	2.37433E − 04
	1	3.26335E − 05	7.71827E − 05
	0.5	1.46031E − 05	3.59437E − 05
0.4	4	3.66029E − 03	4.08557E − 03
	2	8.08060E − 04	9.62798E − 04
	1	1.36048E − 04	3.14642E − 04
	0.5	7.78139E − 05	1.69918E − 04
0.6	4	8.08421E − 03	9.06416E − 03
	2	1.77333E − 03	2.13871E − 03
	1	3.11524E − 04	7.08568E − 04
	0.5	7.50095E − 04	1.64950E − 05
0.8	4	1.38888E − 02	1.56757E − 02
	2	3.02184E − 03	3.70655E − 03
	1	5.52833E − 04	1.25026E − 03
	0.5	1.39851E − 02	3.18297E − 02

Table 2
The L_2 and L_∞ error estimates of numerical solutions with $\tau = 0.01$ and different mesh size computed in *double* precision without using any filter

Time	h	L_2	L_∞
0.2	4	9.07128D − 04	1.00982D − 03
	2	1.99150D − 04	2.37155D − 04
	1	3.17012D − 05	7.73340D − 05
	0.5	1.10894D − 05	3.07712D − 05
0.4	4	3.66214D − 03	4.08854D − 03
	2	8.00849D − 04	9.60164D − 04
	1	1.32570D − 04	3.15757D − 04
	0.5	4.61196D − 05	1.27284D − 04
0.6	4	8.08277D − 03	9.06725D − 03
	2	1.75622D − 03	2.13037D − 03
	1	3.02742D − 04	7.10144D − 04
	0.5	1.08596D − 04	2.94058D − 04
0.8	4	1.38824D − 02	1.56783D − 02
	2	2.99005D − 03	3.69034D − 03
	1	5.39595D − 04	1.25239D − 03
	0.5	2.31716D − 04	5.47905D − 04

3. The filtering method

According to Tikhonov and Arsenin [14], the filtering method of constructing approximate solution of ill-posed evolution problems involves selective perturbation of the initial data so that a good approximate solution can be obtained. The choice of correct amount of perturbation is nontrivial and usually depends on the type of problem and the method used to solve the problem. Since one of the causes of the poor numerical solution here is the growth of spurious perturbations introduced by machine roundoff error, perturbations of the numerical data at various discrete time steps will be chosen here so as to suppress and possibly eliminate the growth of spurious perturbations.

We perturb the data using spectral filters in the following way. The amplitude of nth Fourier mode of a numerical solution before and after the use of a filter $\Phi(n)$ are denoted by a_n and $\tilde{a}_n$ respectively where

$$\tilde{a}_n = a_n \Phi(n). \tag{3.1}$$

Two conventional spectral filters, $\Phi_1(n)$ and $\Phi_2(n)$, that we have used in addition to one more to be constructed and discussed later are>

$$\Phi_1(n) = \begin{cases} \dfrac{a_n - b_n}{a_n}, & n \leqslant n_c, \\ 0, & n > n_c \end{cases} \tag{3.2}$$

and

$$\Phi_2(n) = \begin{cases} \dfrac{|a_n|^2 - |b_n|^2}{|a_n|^2}, & n \leqslant n_c, \\ 0, & n > n_c. \end{cases} \tag{3.3}$$

The cutoff point n_c is the smallest wavenumber with amplitude $a_{n_c} = 10^{-m}$ where m is the computational noise level and is determined by the machine representation of initial condition's Fourier spectrum. Below, we call 'm' the filter level or 'fl' in short. Thus fl = 5 below means that n_c is such that $a_{n_c} = 10^{-5}$. We have performed numerical experiments with various filter levels even though only few cases will be discussed later for conciseness.

These filters set the amplitudes of all modes with wavenumbers $n > n_c$ to zero and modify the amplitudes of all other modes for nonzero values of the parameter b_n in these filters. The choice of b_n should be carefully made so that perturbation of the amplitudes of these modes is minimal and the regularity properties of the filter is as best as possible. The second condition here is an experimental fact which seem to suggest, as we will see below, that better approximate solutions can be obtained with better smoothness properties of the filter in Eq. (3.1). We have performed numerical experiments with following choices of the function b_n: (i) $b_n = 0$, and (ii) $b_n = a_{n_c} + a(n - n_c)$. In the first

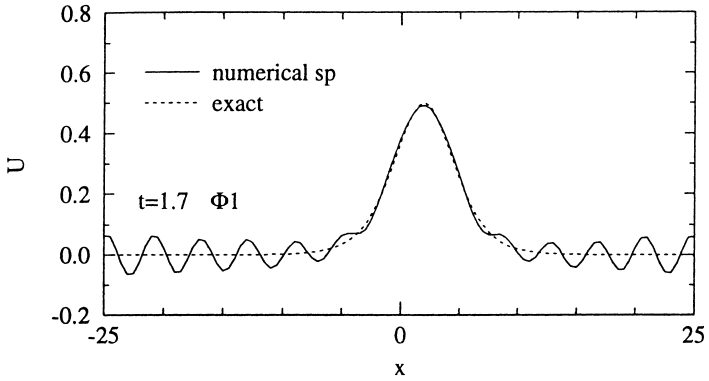

Fig. 6. Comparison of exact solution with the numerical solution obtained by using filter Φ_1 at the time level $t = 1.7$. The calculations were done in single precision (7 digit arithmetics) with $h = 0.5$, $\tau = 0.01$ and filter level 5.

case, $\Phi_1(n) = \Phi_2(n)$ and the effect of these filters is to set the amplitudes of all modes with wavenumbers $n > n_c$ to zero without affecting the other modal amplitudes. Due to this sudden discontinuity in the Fourier spectrum at $n = n_c$, we refer to this filter as 'sharp filter'. Notice that in the second case, i.e. when $b_n = a_{n_c} + a(n - n_c)$, the filter remains continuous but changes the amplitudes of all modes with $n < n_c$ unlike the first case. This change can be kept very small by a choice of very small nonzero values of the coefficient a in the definition of b_n above.

Fig. 6 shows the numerical solution at $t = 1.7$ computed with $\tau = 0.01$, $h = 0.5$ and sharp filter Φ_1 at filter level 5. The numerical solution is compared against the exact solution in this figure. Switching the filter from Φ_1 to Φ_2 in this computation hardly changes the numerical results significant enough to warrant its display. The undesirable oscillations that we see in these numerical solutions with filter Φ_1 or Φ_2 can be eliminated as we will see later with the choice of a more regular filter. Numerous numerical experiments with various levels of these filters and choices of the parameters in these filters indicate that the continuous filter Φ_2 discussed above perform marginally better than the sharp filter in most cases and there is a need for new filters which will allow construction of better approximate solutions than the ones obtainable with these filters.

3.1. The construction of a new filter

The spectrum $\tilde{a}(n)$ given by Eq. (3.1) with $\Phi(n) = \Phi_1(n)$ is a discontinuous function and the one with $\Phi(n) = \Phi_2(n)$ is a continuous function of n for nonzero values of b_n as discussed above. We construct a new filter $\Phi = \Phi_3$

which is twice continuously differentiable and gives a modified spectrum $\tilde{a}_n = a_n \Phi_3(n)$ which is also twice continuously differentiable. This new filter Φ_3 is defined as follows

$$\Phi_3(n) = \begin{cases} 1, & n < n_c, \\ 1 - g(\hat{n}), & n_c < n < n_2, \\ 0, & n > n_2, \end{cases} \tag{3.4}$$

where $\hat{n}$ is defined as

$$\hat{n} = \frac{n - n_c}{n_2 - n_c} \tag{3.5}$$

and the function $g(x)$ which is a $\mathbf{C^2}$ function is chosen as

$$g(x) = \begin{cases} 4.5x^3, & 0 < x < \frac{1}{3}, \\ -9x^3 + 13.5x^2 - 4.5x + 0.5, & \frac{1}{3} < x < \frac{2}{3}, \\ 1 - 4.5(1-x)^3, & \frac{2}{3} < x < 1. \end{cases} \tag{3.6}$$

Even though any $n_2 > n_c$ is allowed, it is preferred that n_2 be within few wavenumbers of n_c. In the equations above, $n_2 \geqslant n_c$ is chosen so that it has the lowest modal amplitude (see Fig. 7(b)). Notice that application of this filter does not change the amplitudes of Fourier modes for $n < n_c$ and the Fourier amplitudes decays monotonically to zero as wavenumber increases from n_c to n_2. Moreover, the modified spectrum is infinitely differentiable everywhere except at $n = n_c$ and $n = n_2$ where it is twice continuously differentiable. Construction of filters with the same properties as Φ_3 except for better continuity properties at $n = n_c$ and $n = n_2$ is straightforward and requires more complicated form of the function $g(x)$. It is helpful to show the Fourier spectrums before and after the application of some of these filters. Fig. 7(a) and 7(b) show the effects of the filters Φ_1 and Φ_3 on the Fourier spectrum of a typical numerical solution at $t = 0.6$. These figures clearly show that these two filters suppress the high wavenumber modes. Logarithmic scale of the ordinate in Fig. 7(a) does not make it possible to show the zero values of all filtered Fourier modes with wavenumber greater than n_c. Our numerical experiments with these filters indicate that computations can be carried out with this new filter Φ_3 for longer time without any undesirable small scale ripples in the numerical solution. In Section 3.2 we present some of these numerical solutions with filter Φ_3.

3.2. Application of the new filter Φ_3

Fig. 8(a) compares the exact solution with the numerical solution at $t = 1$ obtained with the filter $\Phi = \Phi_3$ at filter level 5 in single precision calculation. A comparison of their Fourier spectrums are made in Fig. 8(b). The numerical results shown here have been obtained with mesh spacing sizes $h = 0.5$ and $\tau = 0.01$, the ones also used to obtain the numerical results shown in Fig. 5(a).

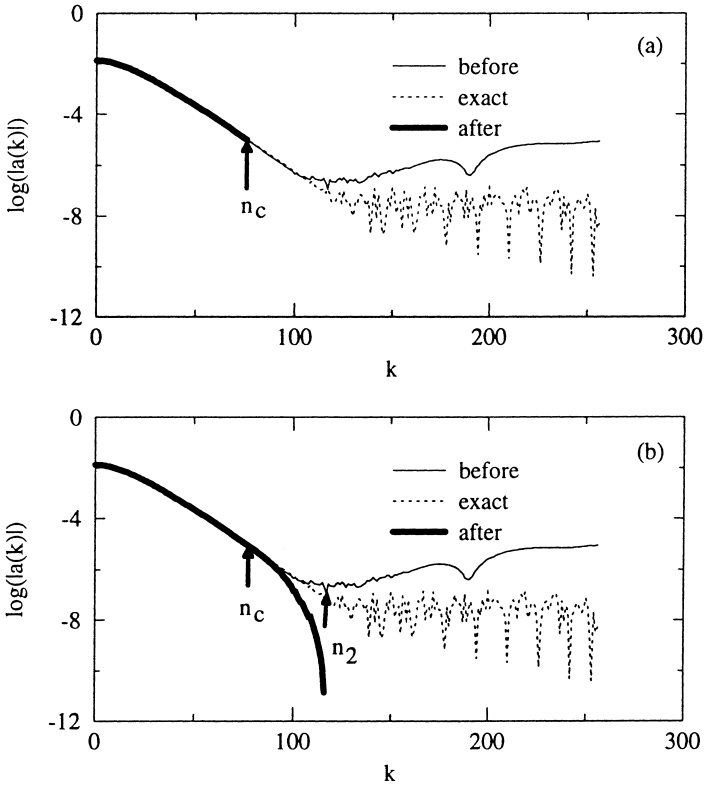

Fig. 7. Effectiveness of the filters (a) Φ_1; (b) Φ_3 in suppressing spurious growth of roundoff errors. Fourier spectra of the numerical solutions at $t = 0.6$ before and after the use of the filters are shown. The computations use $h = 0.5$, $\tau = 0.01$ at filter level 5. The Fourier spectrum of the exact solution is also shown here for comparison purposes.

Comparison of these results with the ones in Fig. 5(a) where no filter is in use shows the effectiveness of this new filter in eliminating the spurious effect of roundoff error.

Fig. 9(a) shows the numerical solution at $t = 1.7$ obtained in double precision calculations with no filter in use. A comparison of this numerical solution with the exact solution in this figure clearly shows the spurious small scale ripples, which is rather severe, in the numerical solution. Fig. 9(b) shows the numerical solution obtained using the filter Φ_3 in single precision at the same time level. These numerical solutions in Fig. 9 should be compared with the numerical solution shown in Fig. 6 which was obtained with the sharp filter Φ_1 at filter level 5 at the same time level. It is quite clear that numerical results obtained with filter Φ_3 are superior to the ones obtained with no filter or with filters of lower order regularity such as Φ_1 or Φ_2.

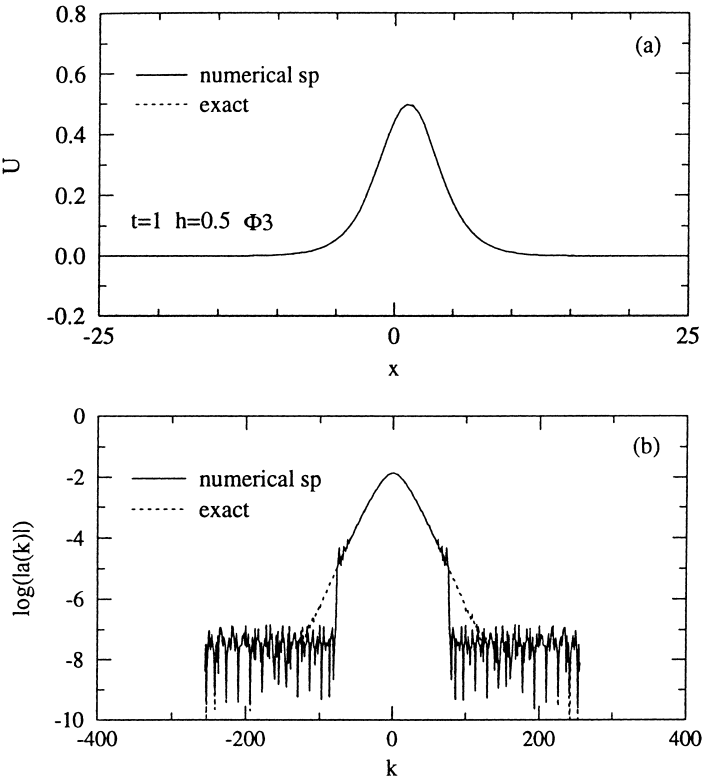

Fig. 8. (a) Comparison of numerical and exact solutions at the time level $t = 1$. The calculations were done in single precision (7 digit arithmetics) with $h = 0.5$, $\tau = 0.01$ and the filter Φ_3 at filter level 5. (b) $\log_{10}|a_k|$ versus k at the same time level where a_k is the Fourier mode with wavenumber k.

It appears from our numerical experiments that smoother filters allow construction of good approximate numerical solutions for longer time. For example, continuation of the numerical solution shown in Fig. 9 for longer time breaks down soon after $t = 4$ due to development of small oscillations. Fig. 10(a) and 10(b) show the numerical solutions at the time level $t = 2$ and $t = 4$, respectively. Small oscillations are evident in Fig. 10(b). In general, it is my contention that better is the smoothness properties of the filter, longer is the time for which the good approximations to the classical solutions of the ill-posed problem can be numerically constructed.

3.3. Effect of filter levels

Through extensive numerical experiments we have found that best approximate solutions with the grid sizes discussed above are obtained with filter

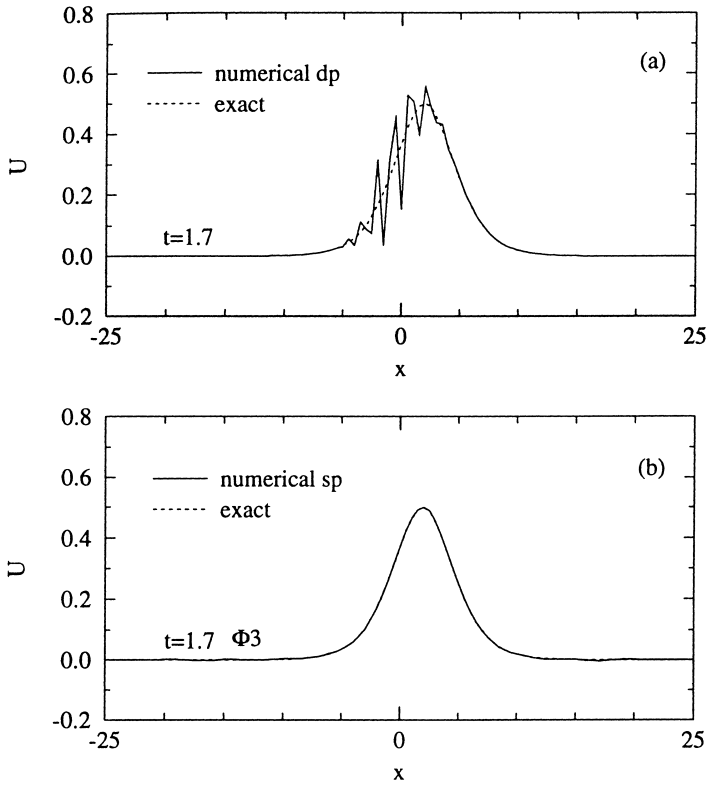

Fig. 9. Comparison of numerical and exact solutions at the time level $t = 1.7$. The calculations were done in (a) *double precision* (15 digit arithmetics); (b) *single precision* (7 digit arithmetics) *with filter* Φ_3 *at filter level 5*. All the computations use $h = 0.5$, $\tau = 0.01$.

level 5 in single precision and filter level 6.5 in double precision. However, double precision calculations with filter level 6.5 are marginally better than with filter level 5. Therefore, calculations with filter level 5 have only been shown. It may seem that use of filter level even higher than 6.5 in double precision calculations should give better solutions for longer time. However, this is not the case here for following reasons.

Usually, a finite number of modes should be sufficient for numerical construction of a good approximate classical solution of the Boussinesq equation. Any attempt to improve the accuracies of the numerical solutions by retaining more than a certain number of modes may actually deteriorate the accuracy of solutions due to catastrophic short-wave instability. Therefore, filter level should be carefully chosen so as to completely suppress nonessential high wavenumber modes. Of course, this is usually difficult without some a priori

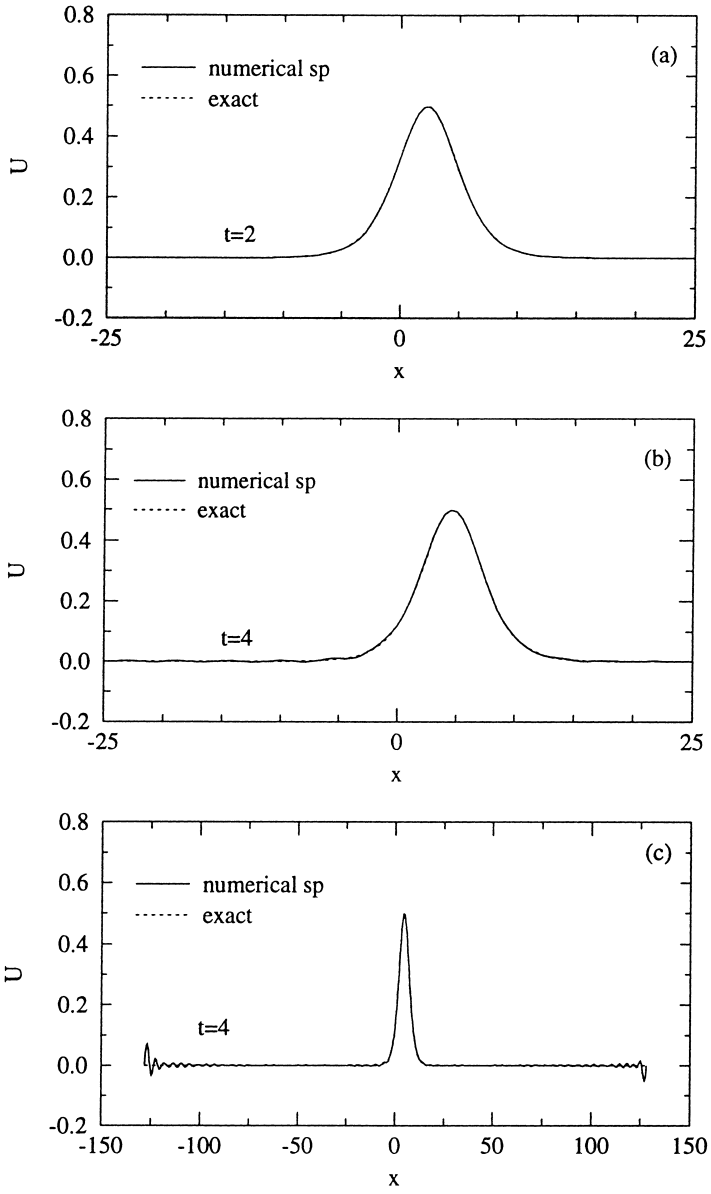

Fig. 10. Comparison of numerical and exact solutions at time levels (a) $t = 2$; (b) $t = 4$. (c) $t = 4$ in the entire computational domain. The calculations were done in single precision (7 digit arithmetics) with filter Φ_3 at filter level 5, $h = 0.5$, and $\tau = 0.01$.

knowledge of the solution itself. In most practical cases, some numerical experiments will be necessary to be able to choose an filter optimal level for best approximate solutions. Finally, it is important to be aware of the fact that filter plays no role unless filter level is larger than the smallest amplitude of the modes participating in the numerical computations. Moreover, it may not always be prudent to choose a filter level closer to the machine precision as this may allow growth of spurious errors in many of the nonessential high wavenumber modes.

4. Regularization methods

We briefly describe two regularization techniques. The Boussinesq equation (1.1) is modified in these regularization techniques by adding appropriate higher order terms to the right-hand side of the equation as discussed below. As we will see below, these modifications do not change the equilibrium states u_c or their characterization as elliptic or hyperbolic states. Therefore, the states with $p'(u_c) < 0$ remain elliptic and states with $p'(u_c) > 0$ remain hyperbolic in these regularized equations.

Below we carry out linearized stability analysis of these regularized equations and derive their dispersion relations. We further argue based on linearized stability analysis and physical consideration that surface-tension-like regularization is more appropriate and is likely to give better approximate solution. Moreover, it is easier here to implement the finite difference scheme with surface-tension-like regularization than with viscosity-like regularization. The numerical scheme of Section 2 is extended below for the regularized equation with surface-tension-like regularization and linearized stability analysis of the scheme is presented. Numerical results with this scheme are then presented. We find that numerical solutions for modest values of regularizing parameters with appropriate filter can provide significantly better approximations to solutions of Eq. (1.1) than the ones obtained by filtering method alone. Below we give more details on these issues.

4.1. First regularization technique

A simple way to regularize is to modify the Boussinesq equation (1.1) as follows,

$$u_{tt} = (p(u))_{xx} + u_{xxxx} + \delta u_{xxxxxx}, \quad \delta > 0. \tag{4.1}$$

Below this equation is referred as MPDE1. The linearized pde corresponding to this regularized equation has decaying as well as growing modes, $e^{\sigma t + ikx}$, with the dispersion relation about the constant state, u_c, given by

$$\sigma_{\mp} = \mp k\sqrt{k^2 - p'(u_c) - \delta k^4}, \quad \delta > 0. \tag{4.2}$$

It follows from this dispersion relation that there are no decaying or growing modes, $e^{\sigma t + ikx}$, unless

$$4p'(u_c)\delta < 1. \tag{4.3}$$

The choice of δ must satisfy Eq. (4.3) so that the dispersion relation (4.2) is qualitatively similar to that for the original Boussinesq equation which has both growing and decaying modes. A simple calculation shows that the equilibrium states, u_c, in the elliptic as well as hyperbolic region are unstable to modes with wavenumbers in the interval (k_1, k_2) where k_1 and k_2 are given by

$$k_{1,2}^2 = (1 \mp \sqrt{1 - 4p'\delta})/2\delta. \tag{4.4}$$

The mode with the highest growth rate has wavenumber $k_m(\delta)$ where

$$k_m^2 = (1 + \sqrt{1 - 3p'\delta})/3\delta. \tag{4.5}$$

Note that $k_m(\delta) \to \infty$ as $\delta \to 0$ which is consistent with the original Boussinesq equation.

Since all modes with wavenumber $k \geqslant k_2$ have zero growth rate, the ill-posedness of the PDE is not present in this regularized equation. In the limit $\delta \to 0$, the MPDE1 reduces to PDE (1.1) and the dispersion relation (4.2) of the MPDE1 reduces to that of the PDE. Therefore we have some confidence that the smooth solutions of the MPDE1 may converge to the smooth solutions of the PDE.

It is worth noting that for a fixed choice of $\delta > 0$, the dispersion relation (4.2) of the MPDE1 is identical to that of the PDE in the long wave ($k \to 0$) approximation and is given by

$$\sigma_{\mp} \approx \mp k\sqrt{-p'(u_c)}, \quad \text{as } k \to 0. \tag{4.6}$$

These long waves travel at a speed $\approx \sqrt{-p'(u_c)}$ regardless of the value of δ in MPDE1. This also follows directly from the PDE and MPDE1 since in this long wave approximation only the first term in these equations is significant. Therefore solutions of the MPDE1 and the PDE will not differ much if the initial data is a long wave perturbation about the constant equilibrium state.

There is only a finite number of modes which actually participate in a numerical calculation. Usually the highest wavenumber, k_n, that participates in a numerical calculation with n grid points is $O(n)$ (approximately $n/4$). Accurate numerical simulation of the regularized Boussinesq equation (MPDE1) is possible if enough grid points are used so that

$$k_n > k^* = \alpha k_m \tag{4.7}$$

for some suitable choice of $\alpha > 1$. A special choice of k^* is k_2. For choice of $k^* \geqslant k_2$, the numerical scheme (2.1) will be able to resolve all modes which are

dynamically important (according to our linearized analysis). It follows from Eqs. (4.5) and (4.7) that

$$\delta > \frac{2}{3}\left(\frac{\alpha}{k_n}\right)^2\left(1-\frac{p'}{2}\left(\frac{\alpha}{k_n}\right)^2\right). \tag{4.8}$$

Eqs. (4.3) and (4.8) give the following allowable values of δ which are dependent on the choice of k^* made in Eq. (4.7),

$$\frac{2}{3}\frac{\alpha}{k_n}\left(1-\frac{p'}{2}\left(\frac{\alpha}{k_n}\right)^2\right) < \delta < \frac{1}{4p'}. \tag{4.9}$$

Allowable values of δ for a choice of $k^* = k_2$ in Eq. (4.7) are given by

$$\left(\frac{1}{k_n}\right)^2\left(1-\left(\frac{p'}{k_n}\right)^2\right) < \delta < \frac{1}{4p'}. \tag{4.10}$$

In Eq. (4.10), right inequality ensures that regularized and ill-posed Boussinesq equations have modes which are qualitatively similar and the inequality ensures that instabilities of the shortest waves which the grid can resolve are mild so that numerical solution is not contaminated with the spurious growth of roundoff error. For a specific choice of δ, left inequality in Eq. (4.10) gives an estimate of the upper bound of the mesh size (mesh size is $O(1/k_n)$). On the other hand, for a fixed mesh size, however small, reliable numerical solution of the regularized equation is possible if $\delta > \delta^*$ where δ^* is the left inequality in Eq. (4.10) which is approximately $(1/k_n)^2$ for small enough grid size or equivalently very large number of grid points. For choices of $\delta < \delta^*$, filtering will be necessary to eliminate the growth of spurious perturbations of short wave amplitudes.

4.2. Finite difference scheme of MPDE1

The MPDE1 (4.1) is solved numerically using extension of the finite difference method discussed in Section 2.1, i.e. in a finite domain, $a \leqslant x \leqslant b$, for $t > 0$ with uniform grid spacing h in x and τ in t. The finite difference approximation to MPDE1 is then given by

$$\begin{aligned}\frac{D_t^+ D_t^- v_j^n}{\tau^2} = \frac{D_x^+ D_x^-(p(v_j^n))}{h^2} + \frac{(D_x^+ D_x^-)^2(v_j^{n+1}+v_j^{n-1})}{2h^4} \\ + \delta\frac{(D_x^+ D_x^-)^3(v_j^{n+1}+v_j^{n-1})}{2h^6},\end{aligned} \tag{4.11}$$

for $\tau > 0$ and $0 < j < N (0 \leqslant j < N$ in case of periodic domain) where $b - a = Nh$. The truncation error is $E(h, \tau) = \mathrm{O}(h^2) + \mathrm{O}(\tau^2)$. Below this Eq. (4.11) is referred as MFDE1. For non-periodic domain we need the same boundary conditions and initialization given in Section 2.1. In addition, we also need two more fourth order accurate boundary conditions since regularized equation is of higher order than the original Boussinesq equation. These two extra boundary conditions for $n \geqslant 0$ are given by

$$\begin{aligned} v(a - 2h, n\tau) = &-12v(a, n\tau) + 16v(a + h, n\tau) \\ &- 3v(a + 2h, n\tau) - 12v'(a, n\tau)h; \end{aligned} \tag{4.12}$$

$$\begin{aligned} v(b + 2h, n\tau) = &-12v(b, n\tau) + 16v(b - h, n\tau) - 3v(b - 2h, n\tau) \\ &- 12v'(b, n\tau)h. \end{aligned} \tag{4.13}$$

The MFDE1 (4.11) is solved in an interval $-128 < x < 128$ as before for various choice of δ and subject to initial data $u^s(x, 0)$ (see Eq. (1.5)) with amplitude of the solitary wave $A = 0.5$. The boundaries are carefully chosen so that they are far away from the support of the solitary wave for the duration of the computation.

4.3. Linearized stability of the MFDE1 about the constant states

Denoting the perturbation about the constant state, u_c, by $\tilde{v}_j^n$, and then linearizing the MFDE1 about this constant state we obtain

$$\begin{aligned} \frac{D_t^+ D_t^- \tilde{v}_j^n}{k^2} = (p'(u_c)) \frac{D_x^+ D_x^- \tilde{v}_j^n}{h^2} + \frac{(D_x^+ D_x^-)^2 (\tilde{v}_j^{n+1} + \tilde{v}_j^{n-1})}{2h^4} \\ + \delta \frac{(D_x^+ D_x^-)^3 (\tilde{v}_j^{n+1} + \tilde{v}_j^{n-1})}{2h^6}. \end{aligned} \tag{4.14}$$

With $\tilde{v}_j^n = \rho^n \mathrm{e}^{\mathrm{i}\xi j}$ in Eq. (4.14). (where $\rho = \mathrm{e}^{\beta\tau}$, $\xi = kh, k$ is the wavenumber and real part of β is the growth rate), the dispersion relation for the numerical scheme is

$$A\rho^2 + 2B\rho + A = 0, \tag{4.15}$$

where

$$A = 1 - 8r^2 \sin^4 \frac{\xi}{2} + 32\delta\theta^2 \sin^6 \frac{\xi}{2}, \qquad B = 2\lambda^2 p'(u_c) \sin^2 \frac{\xi}{2} - 1, \tag{4.16}$$

where $\lambda = \tau/h, r = \tau/h^2$ and $\theta = \tau/h^3$. Numerical scheme (4.11) should preferably use values of grid size τ and h which allow the dispersion relation versus the wavenumber k, best approximate the continuous dispersion relation over as

wide range of the spectrum as possible. Fig. 11 shows the plot of growth rate against the wavenumber k for two values of δ when $u_c = 0$. We have chosen $h = 0.5$ and $\tau = 0.01$ so that numerical results of this regularized equation can be compared with those we have discussed in Sections 2 and 3. It is evident from Fig. 11 that all modes with wavenumber $k \geqslant k_2$ have zero growth rate which completely eliminates the short wavelength instabilities. It is important to notice from Eqs. (4.2) and (4.3) that the constant state $u_c = 0$ is neutrally stable for $\delta > 0.25$. Therefore the dispersion relations in this figure has been shown for choices of $\delta < 0.25$ only.

4.4. Numerical results

We illustrate the effect of regularizing term by presenting numerical solutions of the regularized Boussinesq equation for several values of δ. First we should note from Eqs. (4.4) and (4.5) that most unstable wavenumber k_m and the cutoff wavenumber k_2 are $O(1/\sqrt{\delta})$ as $\delta \to 0$. Moreover, it follows from Eqs. (4.2) and (4.5) that growth rate of the most unstable wave is given by $\sigma(k_m) = O(1/\delta)$ as $\delta \to 0$. Therefore numerical difficulties due to machine roundoff error that we have discussed in Section 2 for the case $\delta = 0$ should also occur for small values of δ when computations are carried out with sufficient number of mesh points. As before, these difficulties for small values of δ can be overcome up to some finite time using either higher precision calculations or filtering techniques. We first provide some calculations when $\delta = 0.05$, $h = 0.5$ and $\tau = 0.01$. For comparison purposes and clarity of exposition of these numerical results, we first show a single precision calculation with $\delta = 0$.

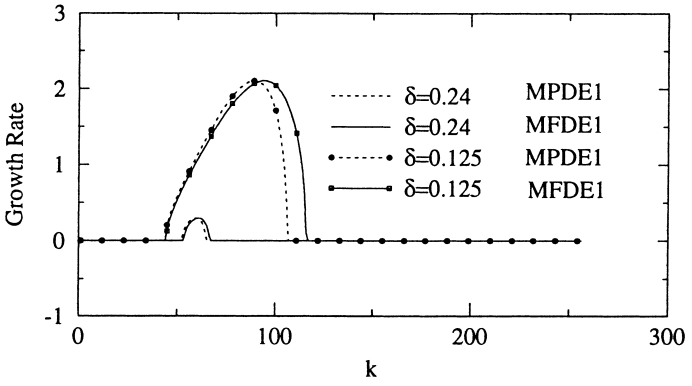

Fig. 11. Dispersion relation for MPDE1 and MFDE1: Growth rate versus wavenumber k for $u_c = 0.0$, $h = 0.5$, $\tau = 0.01$ and two choices of δ.

Fig. 12 compares the computed solutions of the ill-posed Boussinesq equation in 7 digit arithmetics (i.e. single precision) with its exact solutions at two successive time levels. As previously discussed in Section 2, small scale ripples in the computed solution at $t = 1$ in Fig. 12(b) is due to amplification of the amplitudes of short waves spuriously introduced by the machine roundoff error. This is seen in Fig. 12(c) where we have plotted logarithm of the Fourier coefficients' amplitudes against wavenumbers for these computed solutions. It is worth recalling from Section 2 that Fourier coefficients of the initial data (solitary wave) decay monotonically with wavenumber. However we see in Fig. 12(c) that all participating modes with amplitudes smaller than 10^{-7} in single precision calculation are replaced by roundoff error of the order of 10^{-7}. The errors in the amplitudes of these short-waves which are many thousand-fold higher than their correct amplitudes get amplified at later times by the severe short-wave instability causing violent small scale oscillations to appear at $t = 1$ as seen in Fig. 12(c).

Figs. 13 and 14 show the numerical solutions of the regularized Boussinesq equation at successive time levels that were obtained in single and double precision calculations respectively. These computations use $\delta = 0.05,\ h = 0.5$ and $\tau = 0.01$. In these figures, numerical solutions for these time sequences have also been compared with exact solutions of the ill-posed Boussinesq equation. The computed solutions of the regularized equation (4.1) for earlier times have not been shown in these figures because these solutions not only contain no irregularities but also compare very well with the exact solutions $u^s(x,t)$ of the ill-posed equation (1.1).

Very small irregularities that appear in the numerical solution at $t = 1.7$ in Fig. 13(b) is largely due to amplification of spurious perturbation in the amplitudes of short waves introduced by machine round off error and not due to small nonzero value of δ. This is seen in Fig. 13(c) where we have plotted logarithm of the Fourier coefficients' amplitudes against the wavenumbers. We should recall that Fourier coefficients of the initial data decay monotonically with wavenumber. However we see in Fig. 13(c) that all participating modes with amplitudes smaller than 10^{-7} in single precision calculation are replaced by roundoff error of the order of 10^{-7}. The errors in the amplitudes of these short-waves which are many thousand-fold higher than their correct amplitudes get amplified at later times due to their severe growth rate at such a small value of δ. This causes the irregularities in the numerical solution shown in Fig. 13(b). However, these irregularities could have been much worse if it were not for the small value of the regularizing parameter δ. A comparison of the numerical solutions in Figs. 12 and 13 show this. A comparison of the Fourier spectrums of these solutions in Fig. 12(c) and Fig. 13(c) clearly show the effects of nonzero values of δ in reducing the growth rate of the short-wave components of roundoff error and thereby providing better approximate solutions of the ill-posed Boussinesq equation.

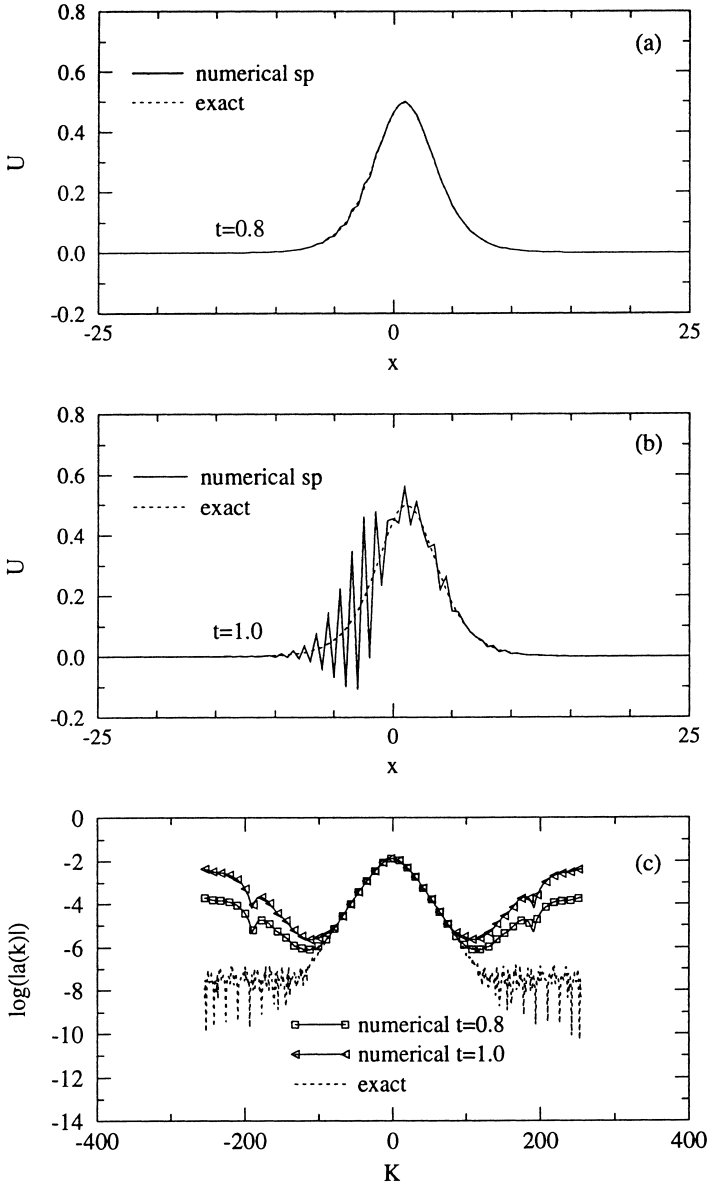

Fig. 12. Computed solutions of the ill-posed Boussinesq equation at time levels $t = 0.8$ and $t = 1.0$. The calculations use $h = 0.5$, $\tau = 0.01$ and were done in single precision (7 digit arithmetics). (c) Logarithm ($\log_{10}$) of the Fourier coefficients' amplitudes against the wavenumber k for the initial data and the computed solutions.

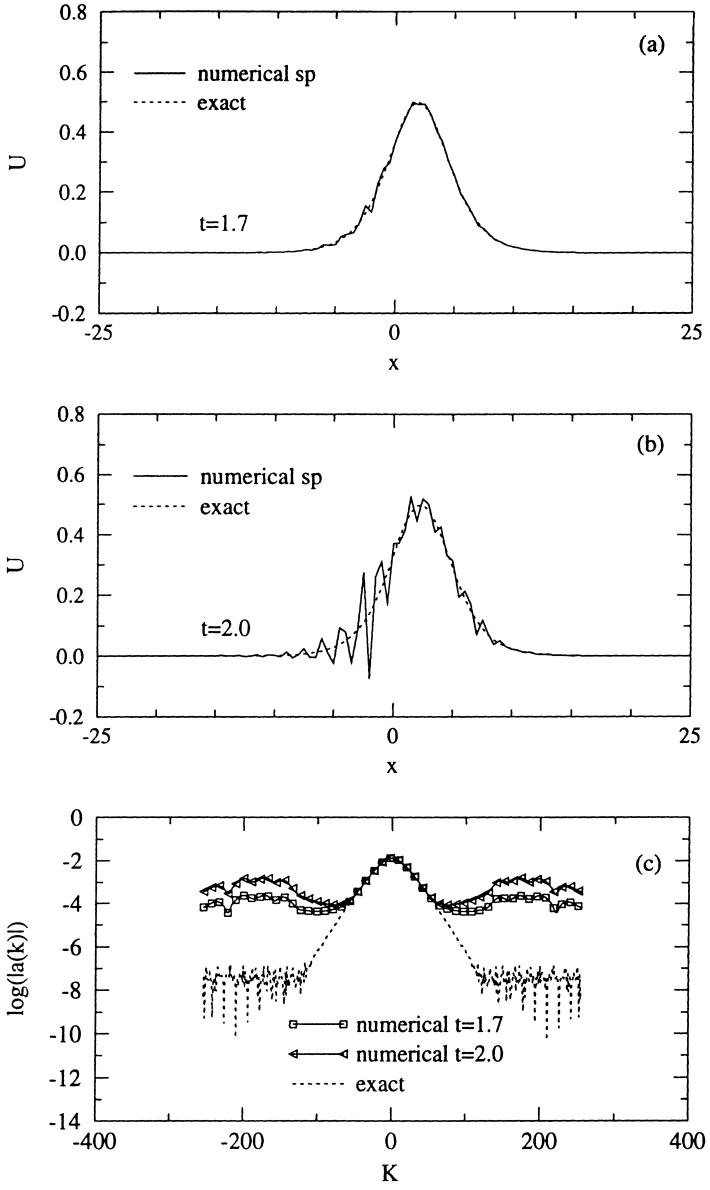

Fig. 13. Computed solutions of the regularized Boussinesq equation at time levels $t = 1.7$ and $t = 2.0$. The calculations use $h = 0.5$, $\tau = 0.01$, $\delta = 0.05$ and were done in single precision (7 digit arithmetics). (c) Logarithm ($\log_{10}$) of the Fourier coefficients' amplitudes against the wavenumber k for the initial data and the computed solutions.

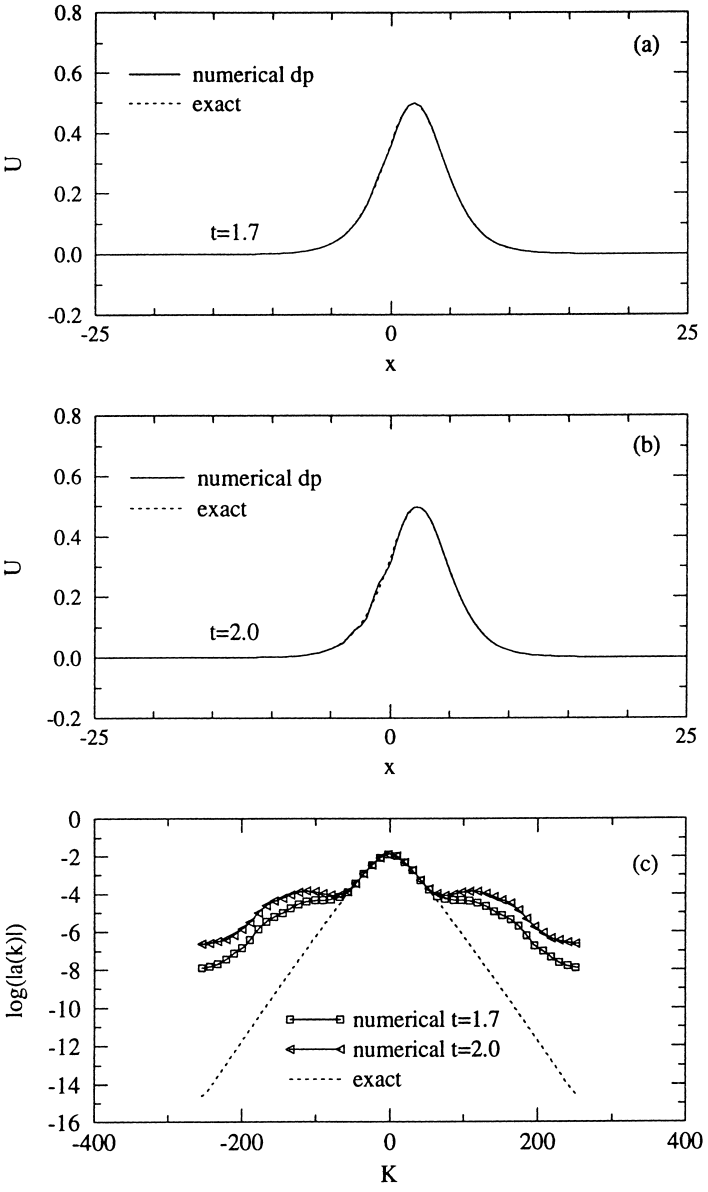

Fig. 14. Computed solutions of the regularized Boussinesq equation at time levels $t = 1.7$ and $t = 2.0$. The calculations use $h = 0.5$, $\tau = 0.01$, $\delta = 0.05$ and were done in double precision (15 digit arithmetics). (c) Logarithm ($\log_{10}$) of the Fourier coefficients' amplitudes against the wavenumber k for the initial data and the computed solutions.

Higher precision calculations provide even better approximate solutions due to less roundoff error. In this regard, single precision calculations of Fig. 13 should be compared with the double precision calculations of Fig. 14 where all participating modes have amplitudes larger than the machine precision and therefore no irregularities appear in the numerical solutions. This further supports our earlier contention that the irregularities of Fig. 13(b) is due to the roundoff error and not due to nonzero value of $\delta = 0.05$. For reasons discussed earlier, effect of roundoff error for even higher precision calculations here is marginal unless computations are carried out on finer mesh sizes.

We have seen in Section 3 that an alternative to using high precision calculations to improve numerical accuracy is to use filtering technique with lower precision calculations. We have experimented with the three filters discussed earlier in Section 3 and have found the filter Φ_3 to perform the best at filter level 5 in single precision calculations. We recall that this filter replaces all the Fourier modes having amplitudes less than 10^{-5} with modified values of amplitudes less than 10^{-5} such that the modified spectrum, i.e. Fourier modes' amplitudes versus the wavenumber curve, is a rapidly decaying C_2 function. Effect of this filter is to set most of these Fourier modes' amplitudes to zero except a very few ones closest to the cutoff wavenumber whose amplitudes rapidly decay to zero from 10^{-5}. Single precision calculations using this filter are shown in Fig. 15. This should be compared with single and double precision results of Figs. 13 and 14. A comparison of the Fourier spectrums of these solutions in these figures show the effectiveness of the filter in suppressing the growth of spurious perturbations introduced by machine precision. Moreover, we see considerable improvements in the accuracy of the computed solutions using this filter.

Numerical experiments for various choices of δ indicate that good approximate solutions of the ill-posed Boussinesq equation can be obtained with rather large values of δ. Fig. 16 shows that numerical solutions with $\delta = 0.25$ are significantly better approximations to the exact solutions of Eq. (1.1) than those we obtained earlier with the filtering technique alone. It is worth recalling that the null state for the regularized equation is neutrally stable exactly at $\delta = 0.25$.

Fig. 17 shows the case when $\delta = 0.125$. Here the numerical solutions at two time levels are shown only. The oscillations in the numerical solution at $t = 4$ in 17(b) quickly grow and does not allow any meaningful solution for later times to be computed. Fig. 18 shows the other extreme when $\delta = 1$. The shift is more severe and oscillations occur at the right-hand side (not left-hand side as we saw in Fig. 17(b)) of the solitary wave. We do not know whether these oscillations are properties of the solutions of the regularized equation or are purely a result of numerical artifacts such as phase error. We do not seek to resolve this issue here and hope to consider this issue in our future work.

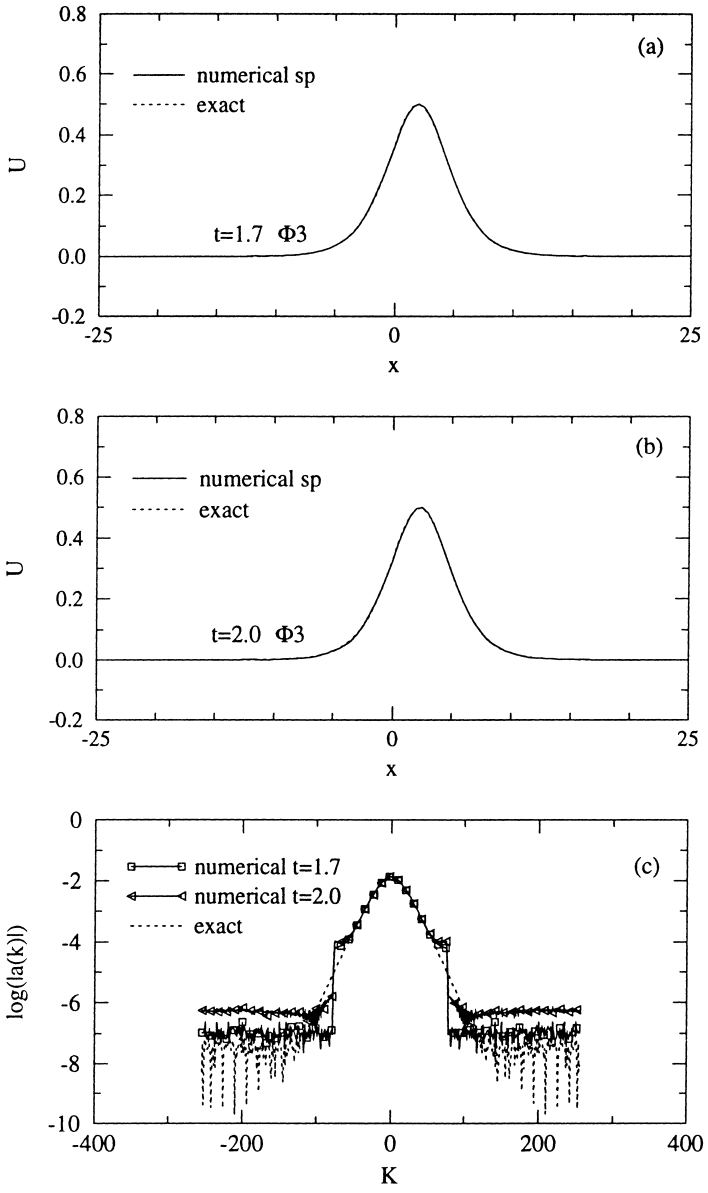

Fig. 15. Effect of the filter Φ_3 on the computed solutions of Fig. 14: single precision (7 digit arithmetics) calculations with filter level at 10^{-5}.

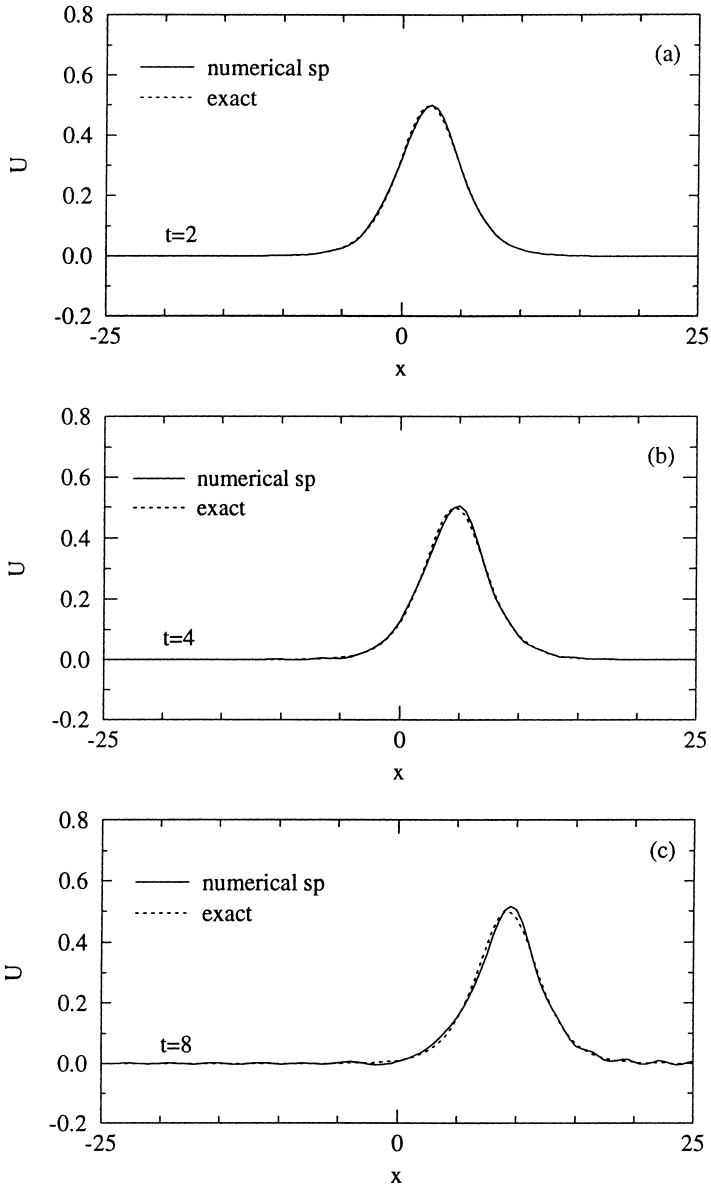

Fig. 16. Comparison of numerical solution of MFDE1 and exact solution of PDE at different time levels (a) $t = 2$; (b) $t = 4$; and (c) $t = 8$. The calculations were done in single precision (7 digit arithmetics) with $h = 0.5$, $\tau = 0.01$ and $\delta = 0.25$.

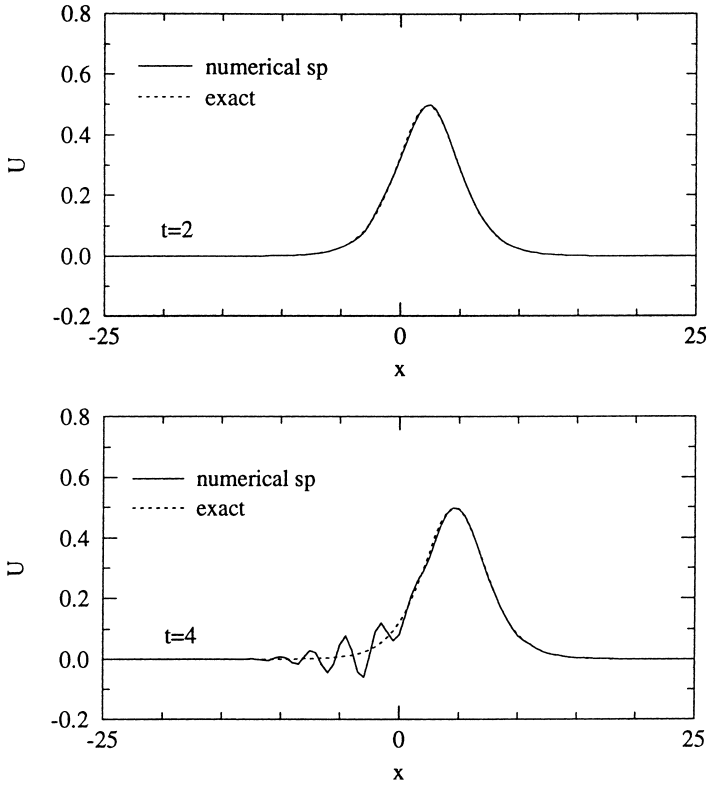

Fig. 17. Comparison of numerical solution of MFDE1 and exact solution of PDE at two time levels (a) $t = 2$; and (b) $t = 4$. The calculations could not be continued upto $t = 8$ (see text). The calculations were done in single precision (7 digit arithmetics) with $h = 0.5$, $\tau = 0.01$ and $\delta = 0.125$.

However, we should notice that these oscillations is the least when $\delta = 25$. Lastly, Table 3 gives error estimates of the numerical solutions of the FDE in double precision, the FDE with the filter Φ_3 at the filter level 5 in single precision and the MPDE1 with three different δ in single precision. For an approximate solution at large times, the MFDE1 with $\delta = 0.25$ appears to be the best choice.

4.5. Convergence issues

The finite difference scheme (4.11) has been numerically tested for convergence with respect to mesh refinement for fixed nonzero values of δ as well as with respect to δ approaching zero for small but fixed values of mesh size. We

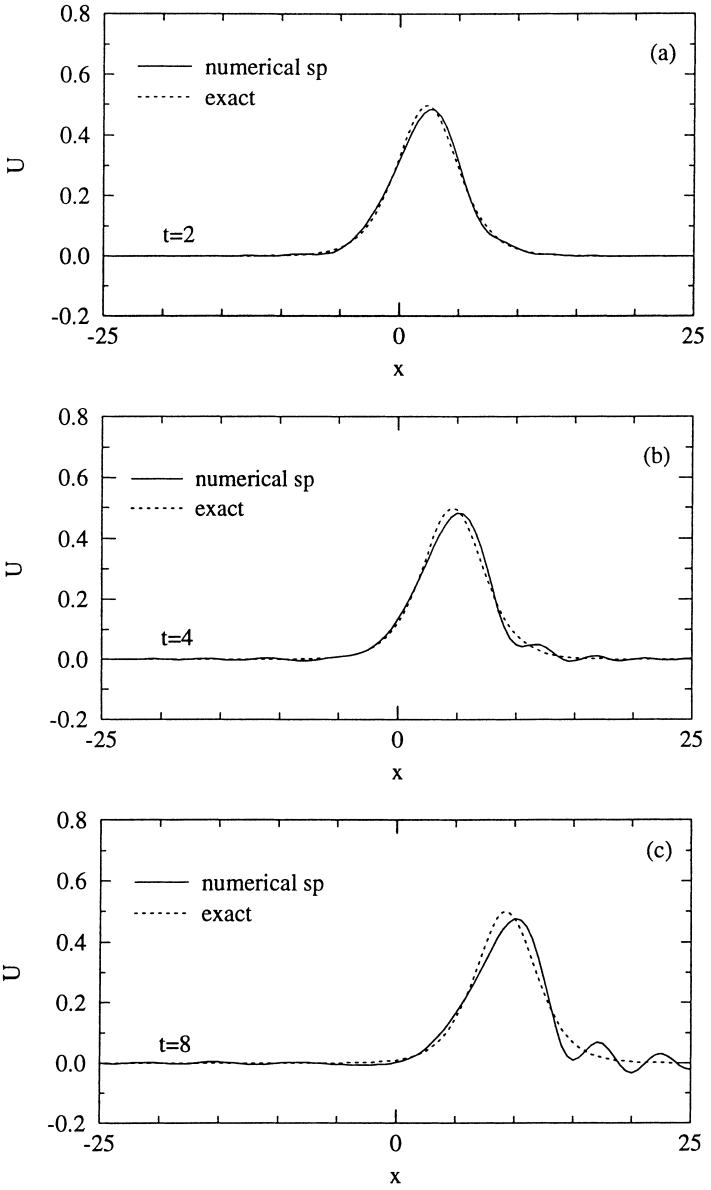

Fig. 18. Comparison of numerical solution of MFDE1 and exact solution of PDE at different time level (a) $t = 2$; (b) $t = 4$; and (c) $t = 8$. The calculations were done in single precision (7 digit arithmetics) with $h = 0.5$, $\tau = 0.01$ and $\delta = 1$.

Table 3
The L_2 and L_∞ error estimates of numerical solutions of the FDE in double precision, the FDE with the filter Φ_3 at the filter level 5 in single precision and the MFDE1 with three different δ in single precision. All calculations were done with $h = 0.5$ and $\tau = 0.01$

Method	Time	L_∞	L_2
FDE (dp)	1.7	0.21603	0.39146
FDE with Φ_3 (sp)	1.7	2.69880E − 03	4.46981E − 03
	2	5.97778E − 03	8.72710E − 03
	4	8.21868E − 02	0.196108
MFDE1 $\delta = 1$(sp)	1.7	2.61988E − 02	7.39563E − 02
	2	2.87347E − 02	8.45163E − 02
	4	4.75305E − 02	0.139917
	8	7.32211E − 02	0.255077
MFDE1 $\delta = 0.25$ (sp)	1.7	1.10226E − 02	2.71939E − 02
	2	1.23671E − 02	3.14813E - 02
	4	1.84338E − 02	4.80555E − 02
	8	2.98752E − 02	8.51296E − 02
MFDE1 $\delta = 0.125$ (sp)	1.7	8.54304E − 03	1.71588E − 02
	2	9.79367E − 03	2.09691E − 02
	4	8.30005E − 02	0.183358

find that the scheme converges with respect to the regularizing parameter as well as with respect to the mesh size.

Fig. 19 shows numerical solutions of the regularized equation at $t = 1$ for various choices of δ. Notice that effect of these large values of δ is very mild on the solution which we observed earlier also. Calculations were done in double precision with $N = 1024$ ($h = 0.25$) grid points and time step $\tau = 0.01$. L_2 error norms of these numerical solutions were calculated with respect to the exact known solitary wave solution of the ill-posed Boussinesq equation (i.e. when $\delta = 0$ in the regularized equation). Fig. 20 shows the plot of this error against δ which shows that numerical solution of the numerical scheme converges as $\delta \to 0$. In this figure, the error at $\delta = 0$ corresponds to the error between the numerical and exact solutions of the ill-posed Boussinesq equation.

Fig. 21 shows numerical solutions of the regularized equation at $t = 4$ for an increasing sequence of number of grid points. Calculations were done in double precision with $\delta = 0.25$ and time step $\tau = 0.01$. L_2 error norms of these numerical solutions for various choice of number of grid points were calculated with respect to the computed solution on the finest mesh which corresponds to $N = 1024$ ($h = 0.25$) here. Fig. 22 shows the plot of this error against N. Figs. 21 and 22 provide sufficient numerical evidence convergence of the numerical scheme under mesh refinement. This has also been tested for few other values of δ.

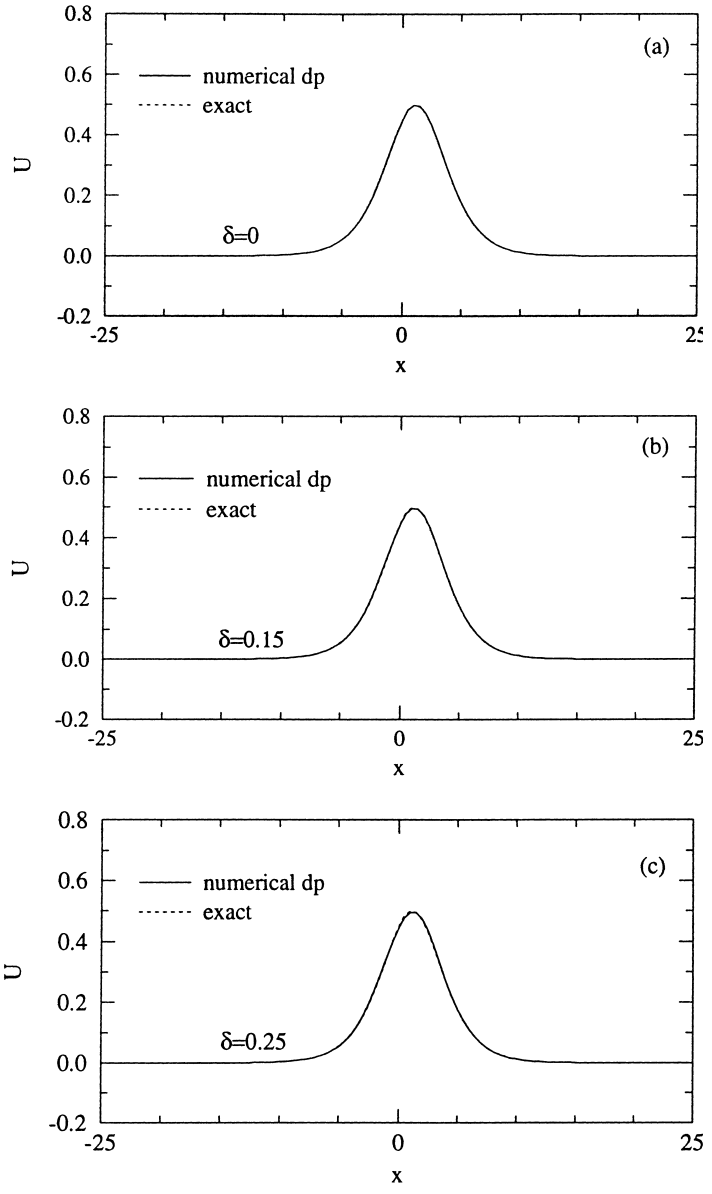

Fig. 19. Solution of the regularized equation at $t = 1$ for $\delta = 0.25, 0.15, 0.0$. Calculations use double precision arithmetics (15 digits), $h = 0.5$ and $\tau = 0.01$.

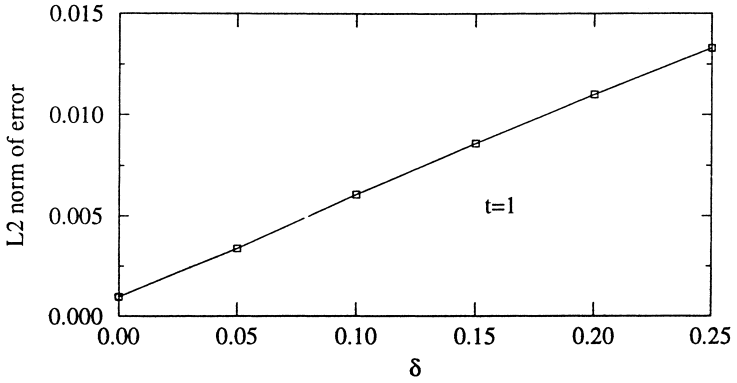

Fig. 20. Plot of the L_2 error norm of the numerical solutions at $t = 1$ against δ. Calculations use double precision arithmetics (15 digits), $h = 0.5$ and $\tau = 0.01$. Errors have been calculated with respect to the exact known solitary wave solution of the ill-posed Boussinesq equation.

4.6. Second regularization technique

For the sake of completeness, it is worth pointing out another regularization technique. The ill-posed Boussinesq equation can also be regularized the following way

$$u_{tt} = (p(u))_{xx} + u_{xxxx} + \delta u_{xxxxxxtt}, \quad \delta > 0. \tag{4.17}$$

We will refer this equation as MPDE2. The linearized pde corresponding to this regularized equation has decaying as well as growing modes, $e^{\sigma t + ikx}$, with the dispersion relation about the constant state, u_c, given by

$$\sigma_{\mp} = \mp k\sqrt{\frac{k^2 - p'(u_c)}{1 + \delta k^6}}. \tag{4.18}$$

Fig. 23 shows the growth rate against the wavenumber for several values of δ and a fixed value of $u_c = 0.0$. The criterion of instability of the equilibrium states, u_c, for this regularized equation is the same as that for the PDE: states in the elliptic region (i.e. $p'(u_c) < 0$) are unstable to all modes and states in the hyperbolic region are unstable to modes $|k| > \sqrt{p'(u_c)}$. It follows from dispersion relation (4.18) that there is a wavenumber $k_m(\delta)$ which has a maximal rate of instability $\sigma(k_m)$ and $k_m(\delta) \to \infty$ as $\delta \to 0$ which is consistent with the original Boussinesq equation. From the dispersion relation (4.18) it follows that for a fixed value of δ,

$$\sigma \sim \mp \frac{1}{k\sqrt{\delta}} \to 0, \quad \text{as } k \to \infty, \tag{4.19}$$

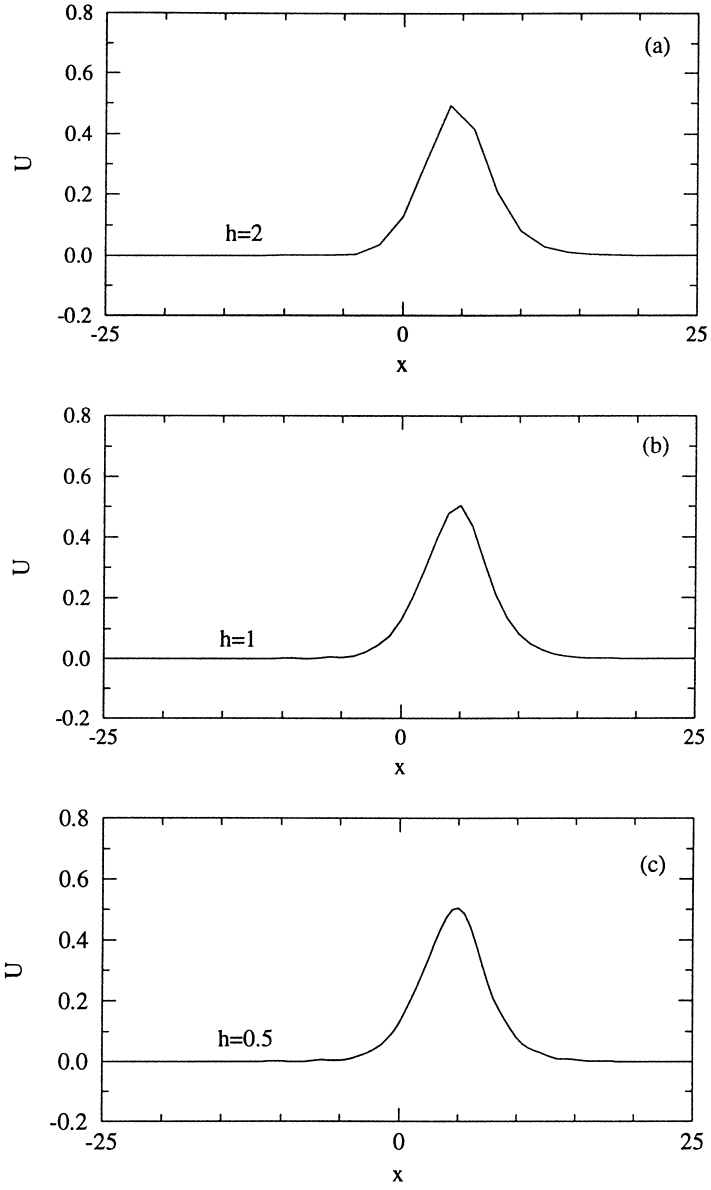

Fig. 21. Solutions of the regularized equation at $t = 4$ for mesh size $h = 2, 1, 0.5$. Calculations use double precision arithmetics (15 digits), $\tau = 0.01$ and $\delta = 0.25$.

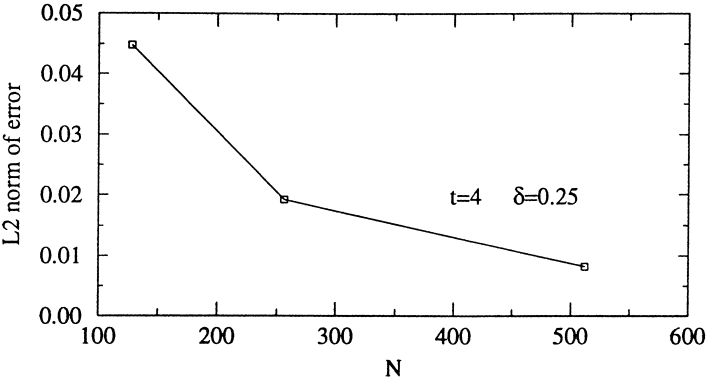

Fig. 22. Plot of the L_2 error norm of the numerical solutions at $t = 4$ against number of grid points. Calculations use double precision arithmetics (15 digits), $\tau = 0.01$ and $\delta = 0.25$. Errors have been calculated with respect to the numerical solution when $N = 1024$.

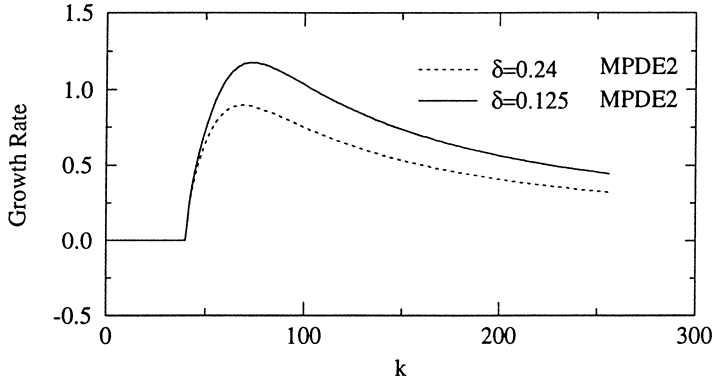

Fig. 23. Dispersion relation for MPDE2: Growth rate versus wavenumber k for $u_c = 0.0$ and two choices of δ.

which removes the catastrophic short-wave instability present in the ill-posed Boussinesq equation (1.1). In the limit $\delta \to 0$, the MPDE2 reduces to the PDE and dispersion relation (4.18) of the MPDE2 reduces to that of the PDE. Therefore we have some confidence that the solutions of the MPDE2 may converge to the solutions of the PDE.

It is worth noting that for a fixed choice of $\delta > 0$, the dispersion relation (4.18) of the MPDE2 is asymptotically identical to that of the PDE in the long wave $(k \to 0)$ approximation. This can also be inferred directly from the MPDE2 since only the first term in this equation is then significant. Therefore

solutions of the MPDE2 and the PDE may not differ much if the initial data are a long wave perturbation about the constant equilibrium state.

If for some suitable $\alpha > 1$, $k_n > \alpha k_m$ is the largest wavenumber that participates in a numerical scheme for a particular choice of δ, then according to the dispersion relation participating short-waves will have small growth rate. Therefore, the numerical scheme will produce numerical solutions which are less likely to be contaminated with machine roundoff error. As $\delta \to 0$, both k_m and k_n approach infinity which may cause catastrophic growth of spurious perturbations if computations are carried out on small enough mesh size. In general, filtering as well as regularization will be necessary for numerical computation of good approximate solutions of the ill-posed equation in the limit $\delta \to 0$.

It is evident from the dispersion relation here that the regularization term in Eq. (4.17) reduces the growth rates of all short waves such that growth rate of short waves vanishes asymptotically which is very reminiscent of the damping usually provided by viscosity in fluid flow contexts. Even though this regularization reduces the spurious effect of roundoff error, it may cause significant attenuation of the solutions, a fact not unusual with viscosity like damping. Therefore, this alternative regularization, even though a viable alternative, is unlikely to be superior to the surface-tension like regularization of the first method we discussed earlier in detail. Hence we have not implemented this method, as mentioned right in the beginning of this section. This regularization method is mentioned here for the sake of discussion and may be implemented by any of the readers, if so desired.

5. Summary

A finite difference scheme for solving an ill-posed Boussinesq equation has been proposed and numerically investigated. The scheme is then used to exemplify the difficulties of computing good approximate solutions of this equation due to catastrophic short-wave instabilities; and to develop appropriate filtering and regularization methods in order to deal with these numerical difficulties. Numerical results indicate that the scheme is convergent and growth of errors can be controlled with suitable filtering and regularization techniques. A rigorous proof of the convergence of the numerical scheme is a topic of future work.

The finite difference scheme that we have proposed here is suitable for studying initial value problems with arbitrary boundary data. However, it may be worth pointing out that this scheme may suffer from some amount of phase error. Spectral filtering technique that we have used here is ideal for periodic data and may require some modification for its use with nonperiodic data

which is as yet another topic of research. For our choices of time and space intervals in the examples presented, the support of solitary wave remains for most examples far away from the boundaries and the data remains periodic within an error of the order of machine precision. Therefore, use of spectral filtering to address issues related to the control of growth of error due to short-wave instability is justified.

Numerical difficulties in computing good approximate solutions can arise due to truncation as well as roundoff errors. We have shown that loss of numerical accuracy is largely due to truncation error when amplitudes of the participating modes are greater than the roundoff error (see Fig. 4). However, roundoff error becomes a major source of numerical difficulty when some of the high wavenumber participating modes have amplitudes much smaller than the roundoff error (see Fig. 5). In this situation, these modes are misrepresented during computation with an amplitude of the order of roundoff error which is significantly higher than the actual amplitudes of these modes in a relative sense. For example, the ratio of roundoff error to the amplitude of the highest participating mode in Fig. 5 is approximately 10^7! A relative error of such a high magnitude gets amplified by the severe short-wave instability during computation resulting in significant loss of accuracy within a very short time. Increasing machine precision can improve the numerical solutions under these circumstances only up to a point until some high wavenumber participating modes attain amplitudes smaller than the roundoff error. Even if the roundoff error is brought under control with high precision arithmetics, the error in the high wavenumber modes due to truncation error which gets amplified significantly by the severe short wave instability of this problem can seriously deteriorate the accuracy of the numerical solution as we have seen in Fig. 4. Finer mesh sizes may reduce the truncation error but may exacerbate the numerical difficulties due to new high wavenumber modes that come into play. Therefore construction of good approximate solutions requires control of both of these types of error.

We have used two common techniques often used in constructing approximate solutions to ill-posed problems: filtering techniques and regularization techniques (see [14]). In filtering technique, the data are appropriately perturbed so that the numerical solution of this modified problem is a better approximation to the solution of the original problem. The practice of perturbing the data by locally averaging the solution in physical space is most common e.g. Rayleigh–Taylor [15], porous media flow [3]. However, the data can also be perturbed by modifying its Fourier spectrum. Most often modification of the data in physical space is somewhat ad hoc and therefore whenever possible, it is preferable to appropriately modify the Fourier spectrum of the data. Moreover, there are at least two advantages to this: (i) spurious oscillations due to the roundoff and truncation errors appear sooner in Fourier space than in physical space allowing earlier control of these errors; and (ii) suitable filters can be

constructed and applied at appropriate filter level to selectively control roundoff and truncation errors. Therefore we have chosen to apply the filtering technique in Fourier space. Use of Spectral filtering technique has also been partly motivated by its success in works of Krasny [7,8] and Shelly [11].

We have experimented with three types of filters with increasing order of regularity and have found that best results were obtained with the filter which is most regular. We introduced a new filter Φ_3 (see Eq. (3.4)) which is a twice continuously differentiable function of the wavenumber k. This new filter has the property that the modified spectrum after its application remains twice continuously differentiable. Choice of filter level is also crucial. With appropriate choice of filter level, filtered computations can be remarkably better than higher precision unfiltered computations (see Fig. 10 and 9(a)). We have found that such an optimal choice of filter level should be somewhat higher (sometime significantly higher as in our double precision calculation where filter level 5 to does better than filter level 12) than the machine precision level. This eliminates many high wavenumber modes which may contaminate the solutions by amplifying roundoff errors in these modes rather than improving the accuracy of these solutions.

In regularization technique the equation, instead of the data, is appropriately perturbed so that the numerical solution of this modified equation is a better approximation to the solution of the original problem. We have shown two ways to perturb the equation by adding a higher order derivative term to the equation. In one approach, it completely eliminates all waves beyond a certain cut-off wavenumber which depends on the small parameter in the highest order derivative term in the equation. This kind of damping is similar to the one usually provided by surface tension. In the other approach, it mildly dampens the growth rate of most waves in such a way that growth rate decays asymptotically to zero with wavenumber. This damping is similar to the one usually provided by viscosity. We have argued in favor of surface-tension-like regularization and extended the finite difference scheme of the original equation for solving the regularized equation with this kind of regularization. The calculations seem to indicate that appropriate choices of parameter values in the regularized equations can provide good approximate solutions of the ill-posed Boussinesq equation at least up to some finite time. Our results indicate that better approximate solutions are obtained with regularization than with filtering technique alone. Regularization with filtering further improves the accuracy of the solutions.

It is worth pointing out that we are not aware of any numerical work on this ill-posed problem. This present numerical work illustrates only some of the difficulties associated with this equation. In closing we should mention some of the interesting problems which may be worth considering as areas of future work: (i) rigorous convergence proof of the finite difference schemes presented in this work; (ii) a study of the structural stability of the solitary wave solution;

(iii) a study of the issues discussed in this paper using other numerical methods such as spectral method; (iv) a systematic numerical study of appropriate initial value problems for the ill-posed and regularized Boussinesq equations; and (v) A numerical study of blow-up and formation of singularities in this equation.

Acknowledgements

The first author (Prabir Daripa) is grateful to Marsha Berger for her hospitality at Courant Institute. P.D. would like to thank Peter Lax and Johnathan Goodman of Courant Institute for sharing their ideas.

Appendix A. Shallow water theory: Long waves

We briefly describe how the ill-posed Boussinesq equation (1.1) arises in the context of water waves. In doing so, we closely follow Chapter 13 of [16]. If time is denoted by t, the space coordinates by (x, y, z), the gravitational acceleration acting in negative y direction by g, the density of fluid by ρ, the pressure in the water by p, the velocity potential in the water by ϕ introduced through the velocity $u = \nabla\phi$ due to irrationality, surface of the water wave by $y = \eta(x, z, t)$, and the bottom of constant depth by $y = -h_0$, then the following equations describe the motion of water in a region Ω subject to an appropriate initial data.

$$\begin{aligned}
&\Delta\phi = 0, \quad \text{in } \Omega,\\
&\frac{p - p_0}{\rho} = -\phi_t - \frac{1}{2}(|\nabla\phi|)^2 - gy, \quad \text{in } \Omega,\\
&\eta_t + \phi_x\eta_x + \phi_z\eta_z = \phi_y, \quad \text{on } y = \eta(x, z, t),\\
&\phi_t + \frac{1}{2}(|\nabla\phi|)^2 + g\eta = 0, \quad \text{on } y = \eta(x, z, t),\\
&\phi_y = 0, \quad \text{on } y = -h_0.
\end{aligned} \tag{A.1}$$

The effect of surface tension has been neglected in the above equations. The linearized version of the above system about an initially rest state of water support waves of the form (see [16])

$$\eta = Ae^{i\boldsymbol{k}\cdot\boldsymbol{x} - i\omega t}, \quad \phi = Y(y)e^{i\boldsymbol{k}\cdot\boldsymbol{x} - i\omega t} \tag{A.2}$$

with the dispersion relation given by $\omega^2 = gk \tanh kh_0$ where k is the magnitude of the wave vector $\boldsymbol{k}$ i.e. $k = |\boldsymbol{k}|$. Therefore the initial value problem associated with the system (A.1) is linearly well-posed.

It should be noted that the dispersive effects drop out in the long wave approximation due to the fact that $\omega^2 \approx gh_0k^2$, as $kh_0 \to 0$ and therefore all long waves in the linear regime travel at the same phase speed $c_0 = \sqrt{gh_0}$. The nondispersive effects in this linear regime within long wave approximation inhibit wave breaking phenomena. Wave breaking phenomena can be captured by incorporating higher order effects of the long wave approximation. One of the ways this is achieved is by setting up a more formal expansion of the system (A.1) in the small parameter $(kh_0)^2$ or equivalently in $(h_0/l)^2$ where l is the wavelength. As derived in [16] in some detail, a nonlinear approximation to system (A.1) which is correct up to the order $O(kh_0)^4$ is given by the following system for one-dimensional waves traveling in the x direction with u being the fluid velocity in this x direction. Below we have used $h = h_0 + \eta$.

$$h_t + (uh)_x = 0, \quad u_t + uu_x + gh_x + \frac{1}{3}c_0^2 h_0 h_{xxx} = 0. \tag{A.3}$$

The linearized version of the system (A.3) about the rest state is given by

$$\eta_{tt} - c_0^2\eta_{xx} - \frac{1}{3}c_0^2 h_0^2 \eta_{xxxx} = 0, \tag{A.4}$$

which has the dispersion relation

$$\omega^2 = c_0^2k^2 - \frac{1}{3}c_0^2 h_0^2 k^4. \tag{A.5}$$

It should be noticed that under the scaling $t \to (h_0/\sqrt{3c_0})t$ and $x \to (h_0/\sqrt{3})x$, Eq. (A.4) reduces to

$$\eta_{tt} = \eta_{xx} + \eta_{xxxx}. \tag{A.6}$$

This is the linearized version of the ill-posed Boussinesq equation (1.1) which incorporates the quadratic nonlinearity of Eq. (A.3).

The dispersion relation (A.5) shows that the system (A.3) is linearly ill-posed and waves with $(kh_0)^2 < 3$ are amplified. To make the study of this equation computationally feasible, an understanding as to how to bring the spurious growth of errors under control as well as some sort of meaningful modification of this equation are required.

One well-posed variants of Eqs. (A.3) and (A.4) favored by Boussinesq [16] are respectively

$$h_t + (uh)_x = 0, \qquad u_t + uu_x + gh_x + \frac{1}{3}h_0 h_{xtt} = 0 \tag{A.7}$$

and

$$\eta_{tt} - c_0^2\eta_{xx} - \frac{1}{3}h_0^2\eta_{xxtt} = 0 \tag{A.8}$$

with the dispersion relation given by

$$\omega^2 = \frac{c_0^2 k^2}{1 + (1/3)k^2 h_0^2}. \tag{A.9}$$

These equations follow directly from the lowest order approximations (e.g. replace η_{xx} by η_{tt}/c_0^2 in Eq. (A.4)) and do not modify the long-wave dispersion relation.

The problem with Eq. (A.8) is that it does not allow, at least in an obvious manner, understanding of Eq. (A.4) or its solutions. Moreover, it has never been shown that the solutions of Eq. (A.8) in any way approximate solutions of Eq. (A.4). It is intuitively more appropriate to regularize Eq. (A.4) in a way that retains its long wave dispersion relation, provides good approximate solutions of Eq. (A.4) when these exist (see Section 4) and provides a hope give to better insight into this equation and its solutions in the some appropriate limit of the regularizing parameter. To achieve these goals it is also essential to explore possible ways, if any, to control the severe growth of numerical errors (see Section 3). Important mathematical issues related to this equation which cannot be answered analytically can possibly then be addressed by computation.

References

[1] M. Affouf, R.E. Caflisch, A numerical study of reimann problems solutions and stability for a system of viscous conservation laws of mixed type, SIAM J. Appl. Math. 51 (3) (1991) 605–634.
[2] G. Baker, D.I. Meiron, S.A. Orszag, Vortex simulations of the Rayleigh-Taylor instability, Phys. Fluids 23 (1980) 1485–1488.
[3] P. Daripa, J. Glimm, B. Lindquist, O. McBryan, Polymer floods: A case study of nonlinear wave analysis and of instability control in tertiary oil recovery, SIAM J. Appl. Math. 48 (1988) 353–373.
[4] P. Deift, C. Tomei, E. Trubowitz, Inverse scattering and the Boussinesq equation, Comm. Pure Appl. Math. 35 (1982) 567–628.
[5] R. Hirota, Exact N-soliton solutions of the wave equation of long waves in shallow-water and in nonlinear lattices, J. Math. Phys. 14 (1973) 810–815.
[6] T.Y. Hou, J. Lowengrub, R. Krasny, Convergence of a point vertex method for vertex sheets, SIAM J. Num. Anal. 28 (1991) 308–320.
[7] R. Krasny, A study of singularity formation in a vortex sheet by the point vortex approximation, J. Fluid Mech. 167 (1986) 65–93.
[8] R. Krasny, Desingularization of periodic vortex sheet roll-up, J. Comput. Phys. 65 (1986) 292–313.
[9] V.S. Manoranjan, A.R. Mitchell, J. Li, Morris, Numerical solution of the good Boussinesq equation, SIAM J. Sci. Stat. Comput. 5 (1985) 946–957.
[10] A.C. Scott, F.Y.F. Chu, D.W. Mclaughlin, The soliton: A new concept in applied science, Proc. IEEE 61 (10) (1973) 1443–1483.
[11] M.J. Shelley, A study of singularity formation in vortex-sheet motion by a spectrally accurate vortex method, J. Fluid Mech. 244 (1992) 493–526.

[12] M. Slemrod, Admissibility criteria for propagating phase boundaries in a van der Walls fluid, Arch. Rational Mech. Anal. 81 (1983) 301–315.
[13] M. Slemrod, Dynamic phase transition in a van der Waals fluid, J. Differential Equations 52 (1984) 1–23.
[14] A.N. Tikhonov, V.Y. Arsenin, Solutions of Illposed Problems, Translated by Fritz John, Wiley, New York, 1977.
[15] G. Tryggvason, Numerical simulations of the Rayleigh-Taylor instabilities, J. Comput. Phys. 80 (1989) 1–16.
[16] G.B. Whitham, Linear and Nonlinear Waves, Wiley, New York, 1974.
[17] V.E. Zhakarov, On stochastization of one-dimensional chains of nonlinear oscillation, Sov. Phys. JETP 38 (1) (1974) 108–110.